MIT Libraries | DSpace@MIT

MIT Open Access Articles

How RO membrane permeability and other performance factors affect process cost and energy use: A review

The MIT Faculty has made this article openly available. ***Please share*** how this access benefits you. Your story matters.

Citation: Okamoto, Yoshiki and John H.Lienhard. "How RO membrane permeability and other performance factors affect process cost and energy use: A review." 470 (November 2019): 114064 © 2019 Elsevier B.V.

As Published: http://dx.doi.org/10.1016/j.desal.2019.07.004

Publisher: Elsevier BV

Persistent URL: https://hdl.handle.net/1721.1/122632

Version: Author's final manuscript: final author's manuscript post peer review, without publisher's formatting or copy editing

Terms of use: Creative Commons Attribution-Noncommercial-Share Alike

Massachusetts Institute of Technology

[1]How RO membrane permeability and other performance factors affect process cost and energy use: A review

Yoshiki Okamoto [a,b], John H. Lienhard [a,*]

[a] *Center for Clean Water and Clean Energy, Department of Mechanical Engineering, Massachusetts Institute of technology, 77 Massachusetts Ave., Cambridge MA, 02139, USA*

[b] *Global Environment Research Laboratories, Toray Industries Inc., 3-2-1 Sonoyama, Otsu, Shiga 520-0842, Japan*

ABSTRACT

Reverse osmosis (RO) technology has progressed steadily over the last few decades. Those gains were achieved through improvements in both RO membrane element performance and energy recovery technologies. However, some recent literature indicates that RO membrane water permeability is approaching performance limits imposed by transport processes and thermodynamic constraints. This paper reviews how RO membrane element performance affects the cost of RO processes, especially the specific energy consumption. RO membrane performance encompasses water permeability, salt permeability, and other some characteristics of the RO element. This paper considers not only conventional RO processes, but also the recently proposed closed-circuit RO and batch RO processes. Even if the membrane water permeability increases, little additional effect is found when the membrane water permeability exceeds around 3 LMH/bar for seawater RO and 8 LMH/bar for brackish water RO in conventional single-stage RO. Increasing membrane water permeability has the potential to decrease membrane surface area and associated costs. A major limitation of most existing literature is that performance is evaluation on in terms of the initial operating conditions. Chronological changes, such as result from fouling, must also be considered to accurately validate how membrane element performance affects RO cost.

Contents

1. Introduction…… 3
2. Models of the RO process…… 6
   2.1. Mass transfer model…… 6
   2.2. Pressure drop and pump work…… 6
   2.3. Thermodynamic model…… 6
3. Conventional RO process…… 7
   3.1. Specific energy consumption…… 7
      3.1.1. RO membrane performance…… 7
         3.1.1.1. Water permeability…… 7
         3.1.1.2. Fouling of the membrane surface…… 11
         3.1.1.3. Salt permeability…… 15
      3.1.2. RO element performance…… 16
         3.1.2.1. Feed side pressure loss…… 16
         3.1.2.2. Permeate side pressure loss…… 16
         3.1.2.3. Feed side mass transfer coefficient…… 17
         3.1.2.4. Fouling to the feed spacer…… 17
         3.1.2.5. Membrane surface area…… 18
   3.2. Cost other than energy…… 18
      3.2.1 RO membrane performance…… 18
      3.2.2 RO element performance and other cost drivers…… 20
4. Closed-circuit RO…… 21
   4.1. Outline of Closed-circuit RO…… 21
   4.2. Energy and cost…… 21
5. Batch RO…… 21
   5.1. Overview of Batch RO…… 21
   5.2. Energy and cost…… 22
      5.2.1. Membrane water permeability…… 22
      5.2.2. Cost…… 23
6. Conclusions…… 23

References…… 24

* Corresponding author.
E-mail address: lienhard@mit.edu (J.H. Lienhard)

Y. Okamoto and J.H. Lienhard, "How RO membrane permeability and other performance factors affect process cost and energy use: A review," *Desalination*, **470**:114064, 15 November 2019.
https://doi.org/10.1016/j.desal.2019.07.004

Nomenclature

Acronyms

BRO	Batch reverse osmosis
BWBRO	Brackish water batch reverse osmosis
BWRO	Brackish water reverse osmosis
CAPEX	Capital expenditure
CCD	Closed-circuit desalination
CCRO	Closed-circuit reverse osmosis
CIP	Cleaning-in-place
ERD	Energy recovery device
LMH	Liters per square meter per hour ($Lm^{-2}h^{-1}$)
MER	Membrane cost relative to energy cost
OPEX	Operational expenditure
PFD	Plug flow desalination
RO	Reverse osmosis
SEC	Specific energy consumption
SWM	Spiral-wound membrane
SWBRO	Seawater batch reverse osmosis
SWRO	Seawater reverse osmosis
TFC	Thin film composite
UF	Ultrafiltration

Symbols

A	Membrane water permeability (A-value) [m^3 m^{-2} s^{-1} Pa^{-1}]
A_m	Membrane surface area [m^2]
a	Correlation factor [-]
B	Membrane salt permeability (B-value) [m s^{-1}]
b	Correlation factor [-]
C_F	Concentration of bulk water in the feed side [kg m^{-3}]
C_f	Foulant concentration of feed water [kg m^{-3}]
C_M	Concentration at membrane surface [kg m^{-3}]
C_P	Concentration in the permeate side [kg m^{-3}]
c	Correlation factor [-]
D	Diffusivity coefficient [m^2 s^{-1}]
d_F	Hydraulic diameter of the feed side path [m]
E_A	Energy required for other accessories [J]
E_{ERD}	Energy recovered by ERD [J]
E_{hp}	Energy required for high-pressure pump [J]
E_{in}	Energy required for intaking feed water [J]
E_{pt}	Energy required for pre and post treatment [J]
E_T	Total energy requirement [J]
f	Fanning friction factor [-]
f_D	Darcy friction factor [-]
J_{crit}	Critical flux for water permeate flux [m^3 m^{-2} s^{-1}]
J_s	Salt permeate flux [kg m^{-2} s^{-1}]
J_w	Water permeate flux [m^3 m^{-2} s^{-1}]
k	Mass transfer coefficient [m s^{-1}]
k_{fp}	Fouling potential factor of feed water [-]
L	Length of feed side path [m]
m_A	Membrane unit price [US\$ m^{-2} h^{-1}]
m_d	Mass of deposited foulants per unit membrane area [kg m^{-2}]
N	Number of stages [-]
ΔP	Transmembrane pressure [Pa]
P_F	Feed side pressure [Pa]
P_P	Permeate side pressure [Pa]
ΔP_F	Feed side pressure loss [Pa]
Q_F	Feed side flow rate [m^3 s^{-1}]
Q_P	Permeate side flow rate [m^3 s^{-1}]
R	Universal gas constant [J K^{-1} mol^{-1}]
R_0	Salt rejection rate [-]
$R_{0,max}$	Available highest salt rejection rate [-]
R_{MEC}	Dimensionless cost factor [-]
Re	Reynolds number [-]
RR	Recovery rate [-]
RR_2	Recovery rate of second pass [-]
RR_t	Recovery rate of total system [-]
Sc	Schmidt number [-]
SEC_{min}	Minimum specific energy consumption [kWh m^{-3}]

SEC_{min}^{norm}	Normalized specific energy consumption at thermodynamic limit [-]
SMC	Specific membrane cost [Pa]
SMC_{min}^{norm}	Normalized specific membrane cost at thermodynamic limit [-]
Sh	Sherwood number [-]
T	Temperature [K]
t	Time [s]
u_F	Velocity of feed side bulk [m s^{-1}]
v_M	Molar volume of feed water at membrane surface [m^3 mol^{-1}]
X_M	Molar fraction of the salt at membrane surface [-]

Greek letters

β	Conversion factor [Pa m^3 kWh^{-1}]
δ	Thickness of boundary layer [m]
ε	Conversion factor [US$ kWh^{-1}]
η_E	Efficiency of ERD [-]
η_P	Efficiency of pump [-]
μ	Viscosity of bulk water in the feed side path [Pa s]
$\overline{\Delta\pi}$	Average osmotic pressure [Pa]
π_F	Osmotic pressure of feed water [Pa]
π_M	Osmotic pressure at membrane surface [Pa]
π_P	Osmotic pressure of permeate water [Pa]
ρ_F	Density of bulk water in the feed side path [kg m^{-3}]

1. Introduction

Water scarcity has been expanding and is expected to keep expanding because of worldwide population growth, especially in developing countries [1-4].

Almost 97% of the water in the world is salty and the remaining is fresh water. However, less than 1% of fresh water is available, and most of the available water in the world presents as either salty seawater or icecaps [1, 5, 6]. The acceptable salinity for drinking water is below 500 ppm, except for special cases in which it may rise to 1,000 ppm [1, 5], and boron concentration is normally limited below 0.5 ppm [7]. Therefore, many regions that lack adequate fresh water resources have turned to desalination of salty to supply drinking water; and other regions are actively discussing this approach.

Desalination technologies can be used to produce an alternative supply of water [2]. The current desalination capacity over the world is about 100 million m^3/d [3]. These systems can be divided into thermal desalination technologies and membrane desalination technologies [2, 3, 8, 9]. About 65% of the total capacity is membrane-based and 31% is thermally driven [3]. The current annual growth rate of membrane desalination in the world is about 55% [3], and the membrane market is estimated to have been about US$30 billion in 2015 [2, 3, 6, 8, 9].

Today, RO membrane technology is the most used desalination technology in the world [3, 10]. RO technology can produce fresh water by applying pressure which is higher than the osmotic pressure of raw water. The raw water source treated by RO may be divided into seawater, brackish water, and others [1, 3, 5, 7-11]. Seawater is the most used feed raw water source accounting for about 57.5% of the desalination capacity contracted between 2015 and June 2018, while brackish water accounts for 18.5% [8, 9].

The RO membrane was developed in 1957 by Reid and co-workers [12]. They developed a cellulose diacetate membrane with salt rejection of membrane up to 96% [12]. In 1960, Loeb and Sourirajan developed an asymmetric cellulose diacetate membrane which showed higher flux and higher salt rejection due to its thin surface [3, 4, 13]. At that point, membrane technology began to see adoption in industrial processes; but the membrane water permeability was only 0.21 L/m^2-hr-bar (LMH/bar) at that time [13].

RO membrane performance generally benefits from having higher permeability, higher selectivity, and higher tolerance to fouling (to avoid flux reduction). In addition, RO membranes should be tough enough to withstand high applied pressures, while they should be thin to make membrane surface area per unit volume as large as possible.

Researchers and manufacturers have improved membrane performance for more than 60 years [3]. Most RO membranes today are thin film composite (TFC) polyamide membranes. TFC membranes have higher water permeability, higher salt rejection, and higher tolerance to broad range of temperature and pH [14]. A TFC membrane is composed of three layers: polyester support layer (100 μm thickness), polysulfonic porous support layer (40-50 μm thickness), and cross-linked aromatic polyamide active layer (0.2 μm thickness), as shown in Fig. 1 [4, 13, 15]. In recent RO membranes, the water permeability (A value) is about 1-2 LMH/bar for seawater RO (SWRO), and 2-8 LMH/bar for brackish water RO (BWRO) [16]. On the other hand, for salt rejection, recent RO membranes exceed 99.7% rejection rate for SWRO [3, 4, 13, 14, 16, 17].

In practical use of RO membranes, the spiral-wound membrane (SWM) element is usually selected as the configuration [11, 18]. The SWM element is composed of RO membrane envelopes, feed spacers, permeate spacers and a permeate center pipe [11, 18-20]. The RO membrane envelopes, feed spacers and permeate spacers are spirally wound around the permeate center pipe, as shown in Fig. 2 [11, 18-21]. In addition, end caps can be equipped at both edges of a SWM element for industrial applications [18]. The SWM element has a good balance between ease of operation, fouling

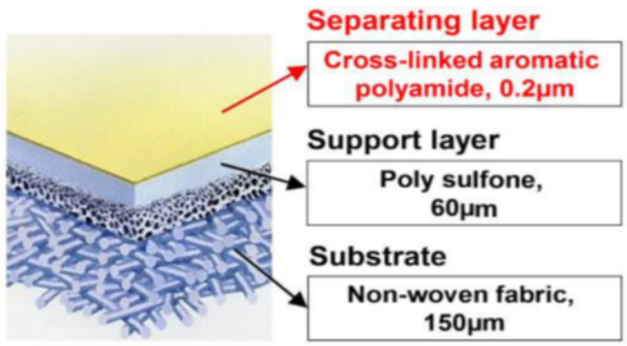

Fig. 1 Structure of composite RO membrane, reprinted from [15].

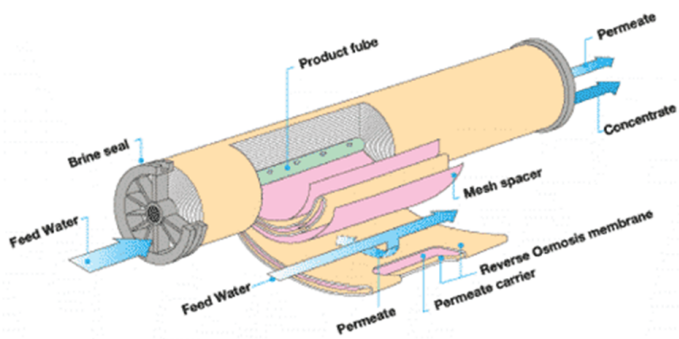

Fig. 2 RO membrane element configuration, reprinted from [21].

control, permeation flow rate, and packing density of membranes [11].

The feed spacer is located between two membrane envelopes so that it faces the active layers of each membrane envelope [5, 11, 19]. The spacer serves to hold the flow path of feed water and to stir the feed water so as to promote mass transfer at the membrane surface. In addition, the feed spacer is designed to make the pressure loss in the feed path as small as possible [5, 11, 19].

The permeate spacer is located inside a membrane envelope to maintain the flow path of permeate water toward the center pipe [5, 11, 19]. This spacer is designed to make the pressure loss in the permeate path as small as possible, but it also should be thin to make the packing density of membranes as high as possible [5, 11, 19].

RO elements are available in several sizes. For industrial application, the SWM elements with diameter of 4, 8, 16 inches (101.6, 203.2, 406.4 mm) are used [11, 19]. The number of membrane envelopes, length, and width of membrane envelopes are designed by a membrane manufacturer. In an industrial RO plant, some RO elements (usually five to eight) are connected in series in an RO module (pressure vessel) [11, 19, 22].

A general industrial RO process is composed of intaking raw water, a pretreatment step, the RO system, a post-treatment step, and water supply pumping [5, 10, 22-29]. The pretreatment step includes sieves, chlorination, coagulation, flocculation, sedimentation, multimedia filtration, cartridge filtration, de-chlorination, and adding acid or anti-scalant [23]. Among these processes, coagulation, flocculation, sedimentation and multimedia filtration can be replaced by ultrafiltration [23]. The RO system is composed of a high-pressure pump, RO modules, and an energy recovery device (ERD) [23]. The post-treatment step includes degassing, remineralization, neutralization and disinfection [5, 10, 22-30].

Conventionally, an RO system has been composed of a single stage as shown in Fig. 3 and Fig. 4 [5, 26, 31]. However, over the last two decades, two-stage RO (Fig. 5) has become to be applied to the RO system instead of single-stage RO to minimize the specific energy consumption, especially for seawater desalination [22, 26, 31-37]. In two-stage RO, concentrated brine from the first stage is further pressurized, to overcome the osmotic pressure of concentrated brine, and then provided to the second stage [26, 31, 32, 34-37]. In addition, permeate two-pass RO processes (Fig. 6) have also been applied to satisfy permeate quality requirements such as lower TDS or boron removal in exchange for an increase of energy and other costs [26, 33, 35, 37, 38]. In the permeate two-pass RO, the permeate of the first pass is pressurized and treated again by second pass RO to decrease TDS or boron concentration [26, 33, 35, 37, 38]. In the case of seawater desalination, the RO elements for second, permeate pass can be elements for BWRO rather than SWRO [22, 33, 35, 38].

As mentioned above, in the case of SWRO, an ERD can be used to reduce the energy consumption [10, 22, 23, 25, 26, 29-32, 35, 39]. By applying an ERD, the specific energy consumption can be decreased by up to 25% [39].

In standard SWRO, the average water permeate flux is within the range of 12-17 LMH, the feed pump pressure is within the range of 55-80 bar, the recovery ratio is within the range of 35-50%, and the system salt rejection is within the range of 99.4-99.7%. On the other hand, in standard BWRO, average water permeate flux is within the range of 12-45 LMH, the feed pump pressure is within the range of 6-30 bar, the recovery ratio is within the range of 50-85%, and the system salt rejection is within the range of 95-99% [7, 23].

The recovery ratio is limited due to increasing energy consumption and scaling risk for SWRO and increasing scaling risk for BWRO [7, 23]. However, in terms of reducing the environmental impact of brine discharge, the recovery ratio of RO process should be increased so that a smaller brine volume is discharged [7, 23].

Water production cost is divided into capital expenditure (CAPEX) and operating expenditure (OPEX) [26, 40-42]. As an example of a typical SWRO plant, CAPEX accounts for about 53% and OPEX accounts for about 47% of the levelized cost of water [26]. In addition, OPEX is divided into three costs including chemical expenses (10%), membrane and filter replacement (21%), and energy consumption (69%) [26, 40-42].

The cost for chemical expenses is related to control of membrane fouling, which decreases water permeate flux as the foulants deposit onto membranes and feed spacers during operation [43-47]. Membrane fouling may be classified into four types: organic fouling, particulate fouling, biological fouling, and inorganic fouling (scaling) [47-49]. Particulate fouling represents the deposition of aluminum silicate, clays,

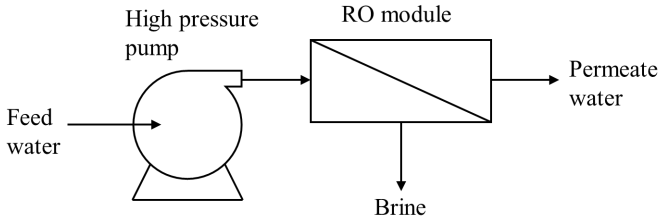

Fig. 3 Single-stage RO arrangement without ERD.

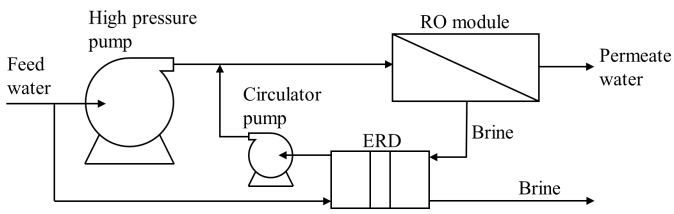

Fig. 4 Single-stage RO arrangement with ERD.

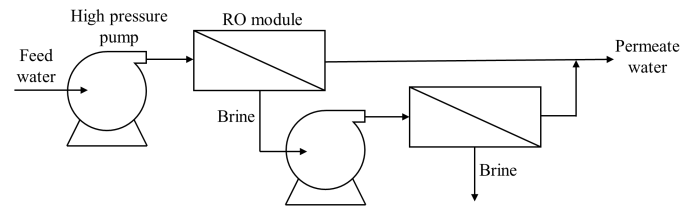

Fig. 5 Two-stage RO arrangement without ERD.

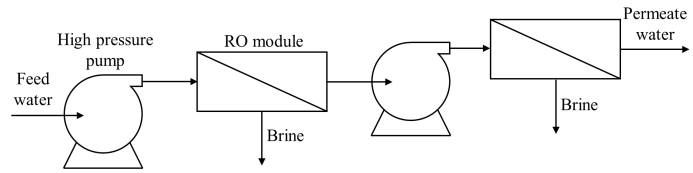

Fig. 6 Two-pass RO arrangement without ERD.

colloids, sand, and silt [47]. Biological fouling represents the deposition of algae and microorganisms, and the growth of bacteria [47]. Organic fouling represents the deposition of polysaccharides, fulvic compounds (fulvic acid and humic acid), and proteins [47]. Inorganic fouling represents the deposition of supersaturated inorganic compounds, such as calcium carbonate, magnesium carbonate, magnesium sulfate, and silica [47, 50].

To clean a fouled membrane, chemical cleaning is conducted once every few months [46, 51, 52]. The frequency of chemical cleaning is determined by the normalized performance of the RO membranes [46]. Cleaning is typically triggered when permeate flow rate or salt rejection decreases by 10% or the feed side pressure loss increases by 15% [23]. A required frequency of chemical cleaning more often than once every three months indicates underperformance of the pretreatment process [23]. Different chemicals are required depending on the type of fouling [45, 46, 53]. Acids are added to remove metallic scales, while alkaline solutions remove biological and organic foulants [45, 46, 54].

Additional operating costs arise from membrane and filter replacement when their performance decreases [55]. In general, RO membrane elements are replaced at a rate of 20% per year for SWRO plants and at 5% per year for BWRO plants [7].

The energy consumption of an RO plant is a major operating cost for SWRO [26]. The total energy requirement when the RO system includes the ERD is expressed by following equation

$$E_T = E_{in} + E_{pt} + E_{hp} + E_A - E_{ERD} \quad (1)$$

where E_T is the total energy requirement, E_{in} is the energy required to intake the feed raw water from the source, E_{pt} is the energy required for pre-treatment and post treatment, E_{hp} is the energy required for high-pressure pump, E_A is the energy required for other accessories (chemical dosing, filter backwashing/cleaning and pumping the permeate fresh water) and E_{ERD} is the energy recovered by the ERD [26]. Energy for the high-pressure pump accounts for 84.4% of the energy consumption in a representative two-stage seawater RO plant [26, 56].

In 1970s, the energy consumption of RO process was high, due to low membrane water permeability and lack of an efficient ERD, and thus the specific energy consumption of RO was as much as 20 kWh/m^3 [10]. However, over 40 years, technological improvements in membranes, elements, pre-treatment options, and development of ERDs, have served to drastically decrease the energy consumption. The minimum specific energy consumption decreased to 8 kWh/m^3 in the 1980s, to 5 kWh/m^3 in the 1990s, and to less than 3.5 kWh/m^3 in the 2000s [10, 57-65]. The water production costs and the specific energy consumption for 20 SWRO plants with water production capacity of greater than 40,000 m^3/d between 2005 to 2010 were within the range of 0.5-3.0 US$/m^3 and 2.5-4.0 kWh/m^3 respectively [22].

In 2014, Cohen-Tanugi et al. [66] indicated that today's RO membrane water permeability is effectively "high enough" and approaching performance limits set by either external mass transfer rates or thermodynamic constraints fixed by the feed and permeate streams. Subsequently, in 2016, a review by Werber et al. [67], highlighted the need for higher membrane selectivity. These studies indicated that improvement of energy efficiency is less likely to be accomplished by increasing membrane water permeability, especially for SWRO.

Since that time, several additional studies of membrane permeability have appeared, and the reported values differ significantly [68-71]. The present review considers all of the past studies and carefully identifies the reasons that they have produced different values of energy consumption.

Beyond that issue, the present review also examines how many additional RO element design factors, other than membrane permeability (A value) or selectivity (salt permeability or B value), affect the process performance and cost. Additional RO element design factors include pressure loss in both feed side path and permeate side path, the degree of concentration polarization, tolerance to fouling, and RO element configuration. These factors have not been considered

comprehensively in previous reviews. Several recommendations for future research directions emerge from this study.

Finally, because research attention has turned toward novel RO configurations, in search of more energy efficient systems, this review considers not only conventional RO process, but also the recently proposed closed-circuit RO and batch RO processes, for both seawater and brackish water desalination.

2. Models of the RO process

2.1 Mass transfer model

Models for mass transfer in the spiral-wound RO membrane element are discussed in the literature [33, 35, 72-88].

Water permeate flux through RO membrane can be expressed, according to solution-diffusion theory, by following equation:

$$J_w = A[(P_F - P_P) - (\pi_M - \pi_P)] \tag{2}$$

where J_w is water permeate flux, A is water permeability of membrane (A value), P_F is pressure in feed side path, and P_P is pressure in permeate side path, π_M is osmotic pressure at feed side surface of the membrane, and π_P is osmotic pressure at permeate side of the membrane.

Salt permeate flux through RO membrane can be expressed, according to Fick's law, by following equation:

$$J_s = B(C_M - C_P) \tag{3}$$

where J_s is salt permeate flux, B is salt permeability of membrane (B value), C_M is salt concentration at membrane surface, and C_P is salt concentration at permeate side of membrane.

Concentration polarization can be expressed by following approximate equation:

$$\frac{C_M - C_P}{C_F - C_P} = \exp\left(\frac{J_w}{k}\right), \qquad k = \frac{D}{\delta} \tag{4}$$

where C_F is the salt concentration of feed side bulk flow, k is the mass transfer coefficient, D is the diffusivity of salt, and δ is the local thickness of the boundary layer. The mass transfer coefficient can be estimated from correlations for Sherwood number as a function of the Reynolds number and Schmidt numbers:

$$Sh = f(Re, Sc) \tag{5}$$

In general, this correlation can be established from experiments. Often, these correlations are developed for a single value of D, so that the dependence Schmidt number is lost [35, 75, 80, 81, 84-88].

2.2 Pressure drop and pump work

Pressure loss in the feed side path is usually expressed by the Darcy-Weisbach equation:

$$\Delta P_F = f_D \frac{\rho_F {u_F}^2}{2} \frac{L}{d_F} \tag{6}$$

where f_D is the Darcy friction factor, ρ_F is density of feed flow, u_F is the velocity of feed side bulk, L is the length of feed side path, and d_F is hydraulic diameter of the feed side path. Fanning friction factor (f) can also be used instead of the Darcy friction factor (f_D) as $f_D=4f$. The Darcy friction factor or the Fanning friction factor are expressed as a function of Reynolds number, which is obtained experimentally [86, 89]. On the other hand, pressure loss in the permeate side path can be expressed by Darcy-Weisbach equation or empirical equations due to the complexity of permeate side spacer configuration.

The specific energy consumption, which is the energy consumption per volume of permeate, is expressed by following equation

$$SEC = \frac{Q_F(P_F - P_P)}{Q_P} = \frac{P_F - P_P}{RR} \tag{7}$$

where SEC is the specific energy consumption, RR is recovery ratio, Q_F is feed flow rate, P_F is feed pump pressure, P_P is permeate side pressure, and Q_P is permeate flow rate [68, 90, 91].

For the RO process, the feed pump pressure must be higher than osmotic pressure at any position in feed side path of RO element. The feed pump pressure is determined by the sum of the brine osmotic pressure (depending on recovery rate, feed salinity, and salt rejection rate), osmotic pressure by concentration polarization (depending on recovery rate, feed side spacer configuration, and permeate flow rate), pressure loss in the feed side path of RO elements (depending on feed side spacer configuration, membrane envelope configuration, recovery rate and permeate flow rate), and additional pressure for permeation (depending on membrane water permeability, arrangement of RO elements, and required permeate flow rate).

2.3 Thermodynamic model

Some studies [5, 30, 61, 66-71, 90-120] have evaluated energy consumption of RO process.

A number of papers [61, 68, 69, 71, 90, 94-99, 109, 114, 115, 119-122] have considered the thermodynamic limit of energy consumption for a conventional single-stage RO process. If a RO membrane element includes an infinitely permeable membrane with perfect salt rejection, but no concentration polarization and no pressure loss, the feed pump pressure has the same value as brine pressure determined by recovery rate and feed salinity only, which is the thermodynamic minimum (limit) feed pump pressure for conventional single-stage RO process. The minimum specific energy consumption for conventional single-stage RO is expressed by following equation

$$SEC_{min} = \frac{\pi_F}{1 - RR} \tag{8}$$

where π_F is osmotic pressure of feed raw water.

Many papers in the literature [68, 94, 97-99, 114, 115] have examined the thermodynamic limit of energy consumption for a multiple-stage RO process. The minimum specific energy consumption is expressed by following equation

$$SEC_{min} = \frac{N(1-(1-RR)^{1/N})}{(1-RR)^{1/N}RR}\pi_F \quad (9)$$

where N is number of stages.

Other literature [98, 99] has considered the thermodynamic limit of energy consumption for closed-circuit RO process. The minimum specific energy consumption is expressed by following equation.

$$SEC_{min} = \frac{2-RR}{2(1-RR)}\pi_F \quad (10)$$

The closed-circuit RO process is described in section **4**.

The thermodynamic limit of energy consumption for an ideal (batch) RO process has been considered in several papers [69, 94, 95, 97, 98]. An ideal RO process does not require additional pressure over osmotic pressure at any position of feed side path in RO modules. The minimum specific energy consumption (i.e., for infinitesimal flux) is expressed by following equation:

$$SEC_{min} = \frac{\pi_F}{RR}\ln\left(\frac{1}{1-RR}\right) \quad (11)$$

The minimum specific energy consumption for a constant finite flux is expressed by following equation:

$$SEC_{min} = \frac{1}{RR}\int_0^{RR}\left(\frac{J_w}{A} + e^{J_w/k}\frac{\pi_F}{1-RR'}\right)dRR' \quad (12)$$

where RR' is the volume fraction of the feed flow rate, recovered as permeate until some intermediate point in the feed side flow path. The ideal (batch) RO process is discussed in section **5**.

In these equations, membrane rejection has been assumed to be perfect, and pump efficiency and ERD efficiency are assumed to be 100%. However, in any real RO plant, many non-ideal factors such as pump efficiency, pressure loss in RO modules and systems, and concentration polarization will act to increase the specific energy consumption as compared to the thermodynamic minimum case.

3. Conventional RO process

The minimum specific energy consumption of SWRO at 50% recovery rate for ideal process is about 1 kWh/m^3 [61, 68, 116, 119]. However, non-ideal factors increase the required energy including those related to RO membrane element performance, such as membrane water permeability, membrane salt permeability, the effect of fouling, pressure loss inside elements, concentration polarization, and other factors such as inefficiency of pumps and other equipment. In addition, for water production cost, fluctuations of the electricity price and plant conditions such as size, configuration, geographic location, raw water property (quality and temperature), water storage and distribution, chemicals, and contracts lead to an increase of water production cost.

In this section, relationships between RO membrane element performance parameters and the cost of water in conventional RO are discussed, especially the specific energy consumption.

3.1 Specific energy consumption

3.1.1 RO membrane performance

There are several parameters in RO membranes which affect the RO membrane element performance. The major parameters are considered, including membrane water permeability, salt permeability and tolerance to membrane fouling.

3.1.1.1 Water permeability

Several studies have evaluated how increasing membrane water permeability decreases the specific energy consumption. Some of them focus on how the specific energy consumption is decreased by replacing an RO membrane element with one that has higher water permeability [66-71, 91, 105-118].

Busch et al. [105] evaluated how the specific energy consumption can be decreased by increasing the total permeate flow rate of a RO membrane element from 28.4 to 34.1 m^3/d, by increasing both membrane active surface area and membrane water permeability. They concluded feed pump pressure would be decreased from 58.3 to 55.8 bar and the specific energy consumption would decrease from 2.27 to 2.17 kWh/m^3 when feed concentration was 38,000 mg/L, recovery ratio was 45%, total permeate flow rate was 9,500 m^3/d, and the number of vessels (each with 7 RO elements connected in series) was 115.

Wilf [106] evaluated how the specific energy consumption of BWRO decreases when replacing RO elements with those having 80% higher membrane permeability. The feed salinity was 1,500 ppm, and the recovery ratio was 85%. He found that specific energy consumption was decreased from 0.52 to 0.40 kWh/m^3 when the average flux was 25.5 LMH, and it was decreased from 0.72 to 0.49 kWh/m^3 when the average flux was 34 LMH.

Franks et al. [107] evaluated how the specific energy consumption decreases when replacing BWRO membrane elements having 34.1 m^3/d of permeate flow by elements having 45.4 m^3/d of permeate flow. The feed pump pressure decreased from 9.8 to 8.3 bar, and the specific energy consumption decreased from 0.41 to 0.35 kWh/m^3. The feed salinity was 1,167 ppm (for wastewater), the recovery ratio was 85%, and the pump efficiency was 83%.

Garg et al. [108] evaluated how the specific energy consumption varies between three RO membrane elements with different water permeability from experimental results for a small-scale brackish-water desalination system; however, the differences of water permeability among the three RO membrane elements were not clearly described.

The results above show that increasing the water permeability of an RO membrane element can decrease the specific energy consumption. This is because an RO membrane element with higher water permeability can reduce the additional pressure over the brine osmotic pressure that is required to get enough permeate water when the average permeate flux is fixed, or it can increase the permeate water flow rate which can raise the recovery rate by increasing the average permeate water flux when the feed pressure was kept fixed. However, in the past ten years, some researchers have indicated that today's RO membrane water permeability is high enough because it is approaching thermodynamic and transport limitations. Even if the membrane water permeability is further increased, the specific energy consumption will hardly be reduced.

Zhu et al. [109] evaluated how improvement of membrane water permeability reduces the water production cost by assessing relationship between the specific membrane cost and the specific energy cost in the case of a purely thermodynamic limit in which pressure loss and concentration polarization in the element are neglected. They modeled the dimensionless cost factor to compare the energy cost with membrane cost. A dimensionless cost factor was defined as a function of feed water salinity, membrane water permeability, the salt rejection requirement of the plant, the cost of electricity, and membrane area. For SWRO, the energy cost was much higher than membrane cost, and they concluded that the highly permeable RO membranes available in 2009 were already near the limit of thermodynamic restriction. They reported little economic incentive for developing higher permeability membranes.

Cohen-Tanugi et al. [66] assessed the benefits gained from ultra-permeable membranes for SWRO and BWRO. For SWRO, feed concentration was assumed as 42,000 ppm, recovery rate was 42%, and salt rejection of membrane was 99.8%. In addition, pump efficiency was assumed as 75% and ERD efficiency was 97%. On the other hand, for BWRO, feed concentration was assumed as 2,000 ppm and recovery rate was 65%. The simulation conditions were shown in Table 1 and 2.

Cohen-Tanugi et al. divided the RO module into several sections along the axial direction and calculated mass transport and fluid flow in each section. The pressure losses on the feed side path were calculated from Fanning's equation, where Fanning friction factor was determined using the formula shown in Table 3. The mass transfer coefficient was calculated according to a correlation of Sh, Re and Sc number which was obtained by fitting data from literature [85] as shown in Table 3. The osmotic pressure was calculated using van't Hoff's law where van't Hoff constant was 2 as shown in Table 3 [123]. The solute rejection rate was assumed as 100%, and pressure loss in the permeate side was assumed as zero.

The results showed that as the membrane water permeability increases, the feed pump pressure decreases asymptotically to the osmotic pressure of brine. For SWRO, increasing membrane water permeability from 1 to 3 LMH/bar decreases the feed pump pressure from 70 to 63 bar, and thus the specific energy consumption is decreased by 15%. However, a further increase of membrane water permeability over 3 LMH/bar does not have any significant effect on reducing the specific energy consumption because 63 bar of feed pump pressure is already within 1% of the osmotic limit for SWRO in this condition. The calculated relationship between membrane water permeability and the specific energy consumption for SWRO is shown in Fig. 7.

On the other hand, for BWRO, increasing membrane water permeability from 1.5 to 4.5 LMH/bar rapidly decreases the feed pump pressure from 12 bar to 6.4 bar. However, a further increase of membrane water permeability does not have much effect, and 5 LMH/bar can be thought as the limit to be effective in reducing the specific energy consumption for BWRO. A calculated relationship between membrane water permeability and the specific energy consumption for BWRO is shown in Fig. 8.

Cohen-Tanugi et al. considered pressure loss on the feed side path and concentration polarization. However, pressure loss in the permeate side path was not considered. Although permeate side pressure loss may be negligible when the feed pump pressure is very high or the permeate flux is low, as the membrane water permeability increases, the permeate side pressure loss may not be negligible due to decreasing feed pump pressure or increasing permeate flux.

Shrivastava et al. [70] evaluated the thermodynamic limit of specific energy consumption by integrating the osmotic pressure inside an RO module for single-stage RO, several-stage RO, and an ideal process which includes infinite stages. They also gave a breakdown of energy consuming parameters in an RO system and how increasing the RO membrane water permeability decreases the specific energy consumption.

Shrivastava et al. considered pressure loss on the permeate side path, and membrane rejection was calculated using salt permeability (B-value) through the membrane. The pressure losses in the feed side path and the permeate side path were calculated using the Darcy-Weisbach equation, where Darcy friction factor was calculated from a correlation of Reynolds number as shown in Table 3 [87]. The mass transfer coefficient was calculated using correlations from the literature [87, 88] as also shown in Table 3. The osmotic pressure was calculated using OLI analyzer 3.1 [124].

For SWRO, the feed concentration was assumed to be 32,000 ppm NaCl, the recovery rate was 50%, the pump efficiency was 85%, and the ERD efficiency was 95% as shown in Table 1. As a result, the potential to reduce the specific energy consumption by increasing membrane water permeability is about 15%. They concluded that if the membrane water permeability is over 4.99 LMH/bar, the effect of increasing membrane water permeability is entirely negligible. The calculated relationship between membrane water permeability and the specific energy consumption for SWRO is shown in Fig. 7.

On the other hand, for BWRO where feed concentration was assumed as 804 mg/L TDS and recovery rate was 85% as shown in Table 2, the potential to reduce the specific energy consumption by increasing membrane water permeability is

about 30%. Thus, there is still room for improvement of energy efficiency by increasing membrane water permeability. However, when the membrane water permeability is still further, the thermodynamic limit is encountered due to the increase of pressure loss, and thus the reduction of specific energy consumption decreases. The calculated relationship between membrane water permeability and the specific energy consumption for BWRO is shown in Fig. 8.

Although these calculations considered pressure losses in both feed and permeate spacers, and concentration polarization, the effect of fouling was not considered. During a plant operation, membrane fouling decreases the water flux, and thus the feed pump pressure must be increased to maintain production, which results in an increase of the specific energy consumption.

Shrivastava et al. also mention the importance of increasing membrane permeability as a goal for future membrane development. General techniques to provide the antifouling property to the membrane are antifouling coating or surface modification. However, these techniques usually reduce the membrane permeability, which may result in increased energy use. Therefore, for the development of membrane with antifouling property, the preservation of highly permeability is still important.

McGovern and Lienhard [69] evaluated how concentration polarization limits the water flux and the specific energy consumption when the membrane water permeability is increased for SWRO. In their model, the mass transfer coefficient of salt at membrane surface in the feed side was assumed as constant (5×10^{-5} m/s), feed seawater osmotic pressure was assumed as 25.6 bar, and the recovery ratio was 50%. Both single-pass and batch RO systems were considered.

McGovern and Lienhard concluded that concentration polarization will limit water flux to roughly 4 times the fluxes typical in seawater systems in 2016 (15 LMH) even if membrane permeability is increased to arbitrarily large values. Further, they note that the limit on flux also creates a lower bound on system size (membrane area) for a given water production requirement. Their work points to the need for higher mass transfer coefficients if high permeability is to become useful.

They also applied this approach to BWRO, concluding that concentration polarization imposes much less of a constraint, with an asymptotic limit on flux that is roughly 20 times today's typical values. Thus, the potential for higher permeability to reduce system size in BWRO is greater.

McGovern and Lienhard also calculated a relationship between membrane water permeability and the specific energy consumption for simple single-pass SWRO system at an average water flux of the system was 15 LMH (shown in Fig. 7). They considered concentration polarization, but did not consider pressure loss inside RO module, fouling, salt permeation, or pump inefficiency. The calculation is essentially a lower bound on energy consumption in this RO configuration.

Werber et al. [67] reviewed module-scale modeling studies and evaluated the impact of membrane water permeability increasing on the process efficiency.

In their model, mass transfer coefficient of salt at membrane surface in the feed side path was assumed as constant (2.77×10^{-5} m/s). Osmotic pressure was calculated by van't Hoff equation where van't Hoff constant is 2 or by using OLI analyzer. The pressure loss inside a RO module was assumed to be zero. For SWRO, feed concentration was assumed as 35,000 ppm NaCl, recovery rate was 50%, and average system flux was 15 LMH. In addition, pump efficiency and ERD efficiency were assumed as 100%, and membrane B-value was used to calculate salt permeability.

They found that increasing membrane water permeability from 0.2 to 1.0 LMH/bar decreases the specific energy consumption by 45% (1.55 kWh/m^3), while increasing membrane water permeability from 10 to 100 LMH/bar yields only 1.0% reduction of the specific energy consumption. Their calculated relationship between membrane water permeability and the specific energy consumption is shown in Fig. 7.

For BWRO, Werber et al. assumed a feed concentration of 5,844 ppm NaCl, and recovery rate was 85%. For a single-stage process, increasing membrane water permeability from 4 to 10 LMH/bar resulted in a 2.2% reduction of the specific energy consumption. On the other hand, for two-stage RO where required energy at 4 LMH/bar of membrane water permeability was 22% lower (0.11 kWh/m^3) than single-stage RO, increasing membrane water permeability from 4 to 10 LMH/bar decreases the specific energy consumption by 12% (0.05 kWh/m^3) which is slightly larger than single stage BWRO. One reason increasing membrane water permeability resulted in only a minor reduction of the specific energy consumption (<0.06 kWh/m^3) is that the hydraulic overpressure is already small. The hydraulic pressure in their single-stage SWRO with 2 LMH/bar membrane water permeability was only 7.6% above the brine osmotic pressure. Their calculated relationship between membrane water permeability and the specific energy consumption is shown in Fig. 8.

Mazlan et al. [68] evaluated the potential for improving membrane water permeability to reduce the specific energy consumption while considering the effect of pretreatment stages and pressure loss on the feed side path for SWRO.

A total permeate water flow rate was assumed as 16,000 m^3/d, a medium sized desalination plant. A typical 8-inch by 40-inch element was selected for the simulation. The feed side pressure loss was calculated using the Darcy-Weisbach equation, where the Darcy friction factor was calculated from a correlation that accounted for the pressure losses in feed tubes and module fittings as shown in Table 3 [86, 89]. Pressure loss in the permeate side path was assumed to be negligible. The mass transfer coefficient was assumed constant (4×10^{-5} m/s), and osmotic pressure was calculated using corrected van't Hoff equation shown in Table 3 [125]. Feed concentration was assumed as 35,000 mg/L, recovery

rate was 50%, average system flux was 22.9 LMH, and NaCl rejection was 100%.

As a pretreatment, a UF membrane was assumed, with 100% permeability for NaCl. The energy consumed by the pretreatment stage was included in the specific energy consumption. The calculated energy consumption for the UF unit was ~0.11 kWh/m^3, and taking account into other pretreatment stages, the total calculated energy consumption for the pre-treatment stage is 0.25 kWh/m^3, which is equivalent to ~13% of that used in RO.

As a result, they suggest that beyond a membrane permeability of approximately 9.72 LMH/bar the specific energy consumption decrease, as a result of thermodynamic limits and concentration polarization. Their calculated relationship between membrane water permeability and the specific energy consumption is shown in Fig. 7.

Shi et al. [110] evaluated the effect of increasing membrane water permeability on achieved system permeability by simulating the performance of an RO element based on the results of experiment conducted in cross-flow cells.

To investigate whether an ultra-permeable membrane can lead to a high flux process, a continuous RO desalination process using a single 8-inch by 4-inch element was studied. Feed side and permeate side pressure losses were calculated using Darcy-Weisbach equation, and the Darcy friction factor was calculated using a correlation from the literature as shown in Table 3 [86]. The mass transfer coefficient of salt at membrane surface in the feed side was calculated using correlation of Re and Sc from other literature [86] as shown in Table 3.

Feed concentration was assumed as 35,000 ppm NaCl, and salt rejection was assumed as 100%. As a result, increasing membrane water permeability shows negligible benefit for the process productivity when the membrane water permeability is over 5 LMH/bar due to the limitations by the concentration polarization and pressure loss in the modules.

The simulation of Shi et al. assumed that increasing membrane water permeability leads to an increase of system flux, but in a real plant, increasing the system flux raises the membrane fouling rate. Therefore, membrane fouling should be considered in the model if the operation with increased flux is assumed.

Wei et al. [126] evaluated the specific energy consumption savings achieved by two-stage BWRO system at various recovery rates with high permeable membranes (3 and 10 LMH/bar) relative to a system with permeability of SWRO membranes nowadays (1 LMH/bar). In addition, they evaluated how the feed salinity affects the specific energy consumption savings when the membrane water permeability increases.

Feed side pressure loss was calculated using Darcy-Weisbach equation, where Darcy friction factor was calculated from a correlation of Re as shown in Table 3 [84, 86]. The mass transfer coefficient of salt at membrane surface in the feed side was calculated using a correlation of Re and Sc number from other literature [84, 86]. Osmotic pressure was calculated from Pitzer equation [127, 128]. Feed concentration was assumed as 3,000 ppm NaCl, and the recovery rate was assumed within the range of 60-98%.

As a result, at low recovery rate, the specific energy consumption saving achieved by 10 LMH/bar of membrane water permeability is quite small (0.02 kWh/m^3 at 60% recovery rate). On the other hand, at very high recovery rate close to saturation (>98%), energy savings are nearly the same regardless of different membrane water permeabilities. The specific energy consumption savings gained by increasing membrane water permeability peaks at 91% of recovery rate. They explained that increasing membrane water permeability from 3 to 10 LMH/bar does not significantly improve energetic performance due to growing of concentration polarization. On the other hand, as for the effect of feed salinity, they concluded that the energy savings obtained by increasing membrane water permeability diminishes as feed salinity increases.

Karabelas et al. [91] assessed how each parameter in RO process such as membrane water permeability (resistance), pressure loss inside the element, osmotic pressure, concentration polarization, pump efficiency, and ERD efficiency affected the specific energy consumption, though they did not show a relationship between membrane water permeability and specific energy consumption directly.

In their simulation, the permeate side pressure loss was calculated using the permeability coefficient which was experimentally obtained in literature [129].

For SWRO, feed concentration was assumed to be 40,000 ppm, the recovery rate was 50%, the feed pump efficiency was 85%, and the ERD efficiency was 95%. As a result, increasing membrane water permeability has the potential to reduce the specific energy consumption by 24.2%.

On the other hand, for BWRO, feed concentration was assumed to be 2,000 ppm, and the recovery rate was 70%. As a result, increasing membrane water permeability has the potential to reduce the specific energy consumption by 51.2%.

Table 1 summarizes the simulation conditions for feed concentration, recovery rate, average system flux or average TMP, number of elements per vessel, salt rejection, pump efficiency, and ERD efficiency of each reference for SWRO. Table 2 provides the same information for the BWRO studies. Table 3 summarizes the models used in each reference for what is considered about variations inside the element, pressure loss in the feed side path and the permeate side path, feed side mass transfer coefficient, osmotic pressure and chronological change such as fouling. Table 4 summarizes the conclusions in each reference about relationship between membrane water permeability and the specific energy consumption for single-stage SWRO, and Table 5 does this for BWRO.

As seen in Fig. 7, the variation of membrane water permeability and the specific energy consumption were a little different among the five studies shown. This results mainly from differences in the model and conditions as listed in Table 3, especially the result by Cohen-Tanugi et al. which considered a much higher feed concentration and a lower

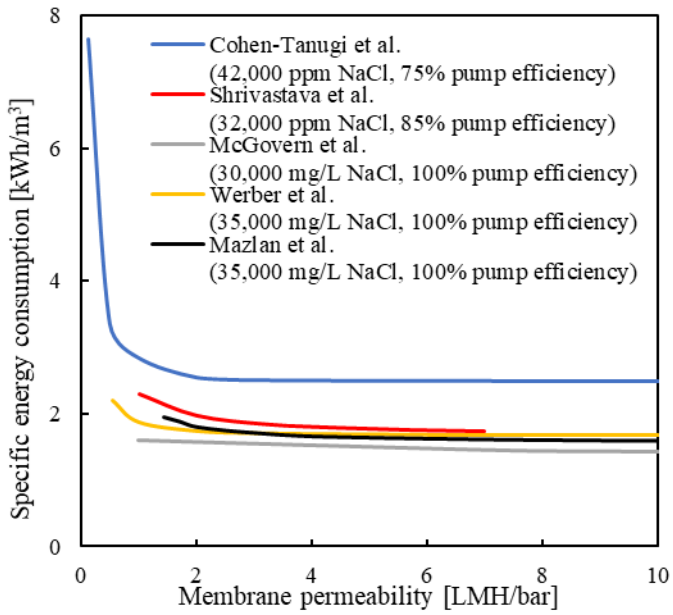

Fig. 7 Calculated specific energy consumption as a function of membrane water permeability for single-stage SWRO from several references at different conditions [66- 70].

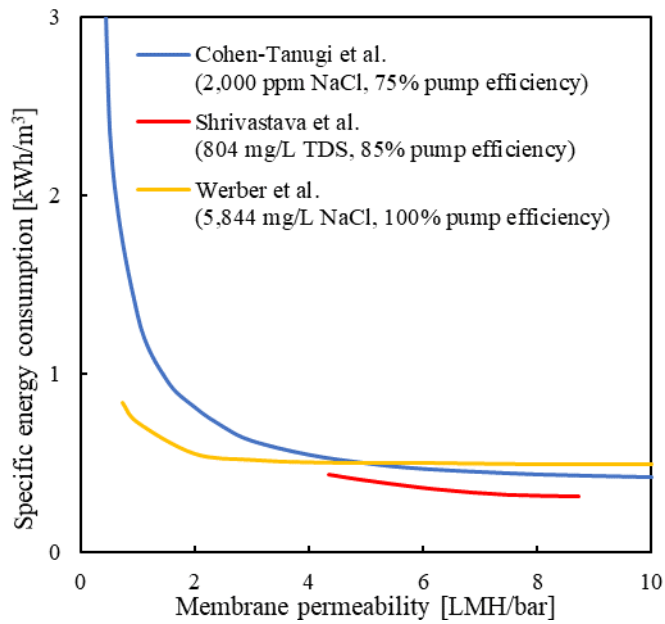

Fig. 8 Calculated specific energy consumption as a function of membrane permeability for BWRO from several references [66,67,70].

pump efficiency. However, in all cases, the specific energy consumption approached an asymptote as the membrane water permeability increased, and negligible reduction in energy consumption when the membrane water permeability exceeded about 3 LMH/bar.

On the other hand, for BWRO, shown in Fig. 8, the relationship between membrane water permeability and the specific energy consumption differs among the three references. This is thought to be due to simulation condition differences about feed concentration, recovery rate, pump efficiency, average system flux and model equations used. In particular, the lower pump efficiency and recovery rate of Cohen-Tanugi et al. cause the higher specific energy consumption when the membrane permeability is low. Although there is no doubt that the rate of reduction in specific energy consumption decreases as membrane water permeability increases, the rate of decrease varies depending on process conditions such as feed salinity, recovery rate, pump efficiency and so on. However, in all cases, energy reduction is negligible if the membrane water permeability exceeds around 8 LMH/bar.

These constraints are due to themodynamic and transport limitations. Specifically, the membrane water permeability of 3 LMH/bar for SWRO and 8 LMH/bar for BWRO lead to downstream conditions with hydraulic pressure only slightly higher than the brine osmotic pressure, as determined by feed osmotic pressure and the recovery rate.

Since the chronological change of RO element performance due to fouling was not considered in any of these studies, these results show the relationships between membrane water permeability and the specific energy consumption at the initial operating condition. However, in real plant operation, fouling decreases the permeate water flux over time, and thus increases the necessary feed pump pressure and the specific energy consumption over time.

Therefore, it is essential to consider chronological changes to accurately evaluate how RO membrane water permeability affects the specific energy consumption and whether higher permeability has an overall benefit.

3.1.1.2 Fouling of the membrane surface

As mentioned in 3.1.1.1, the water permeate flux varies during operation due to fouling which occurs on the membrane surface and the feed spacer. Fouling decreases the permeate flux and thus the feed pump pressure must be increased to keep producing the same flow rate of permeate water. Therefore, to predict the specific energy consumption accurately over time, it is important to consider chronological factors such as fouling or ageing.

Jeong et al. [130] implemented a numerical simulation that considered the effect of fouling. They studied the effects of colloidal fouling employing a cake filtration model. In the cake filtration model, the total membrane resistance was calculated by adding the transient hydraulic resistance of the cake layer. The resistance of the cake layer was estimated using Kozeny-Carman equation. The deposition rate of foulants onto the membrane surface was calculated considering the difference between water permeate flux and critical flux, as expressed in the following equation:

$$m_d = k_{fp} \int_0^t c_f (J_w - J_{crit}) dt \tag{13}$$

where m_d is the mass deposition of foulant to the membrane surface, k_{fp} is the fouling potential factor of feed water, c_f is the fouling concentration of feed, J_w is the permeate water flux, J_{crit} is the critical flux. The attachment of colloid foulants was

Table 1. Simulation conditions of each reference that includes the relationship between membrane water permeability and SEC for SWRO.

Reference	Author (Year)	Condition						
		Feed concentration	Recovery rate	Average system flux/ Average TMP	No. of elements per vessel	Salt rejection	Pump efficiency	ERD efficiency
		ppm or mg/L	%	LMH / bar	-	%	%	%
[109]	Zhu et al. (2009)	35,000 mg/L TDS	50	-/15.5	N.D.	99	100	100
[66]	Cohen-Tanugi et al. (2014)	42,000 ppm NaCl	42	16/-	8	99.8	75	97
[70]	Shrivastava et al. (2015)	32,000 ppm NaCl	50	N.D.	N.D.	N.D.	85	95
[69]	McGovern et al. (2016)	30,000 mg/L NaCl (π_F=25.6 bar)	50	15/-	Not considered	100	100	100
[67]	Werber et al. (2016)	35,000 mg/L NaCl	50	15/-	N.D.	B-value was used	100	100
[68]	Mazlan et al. (2016)	35,000 mg/L NaCl	50	22.9/-	8	100	100	100
[110]	Shi et al. (2017)	35,000 mg/L NaCl	N.D.	N.D.	N.D.	100	N.D.	N.D.
[111]	Wei et al. (2017)	35,000 ppm NaCl	70	15/-	8	100	100	100
[91]	Karabelas et al. (2018)	40,000 ppm	50	N.D.	N.D.	N.D.	85	95

Table 2. Simulation conditions of each reference that includes the relationship between membrane water permeability and SEC for BWRO.

Reference	Author (Year)	Condition						
		Feed concentration	Recovery rate	Average system flux/ Average TMP	No. of elements per vessel	Salt rejection	Pump efficiency	ERD efficiency
		ppm or mg/L	%	LMH/bar	-	%	%	%
[109]	Zhu et al. (2009)	3,500 mg/L TDS	50	-/1.55	N.D.	99	100	100
[66]	Cohen-Tanugi et al. (2014)	2,000 ppm NaCl	65	13.2/-	7	99.8	75	97
[70]	Shrivastava et al. (2015)	804 mg/L TDS	85	N.D.	N.D.	N.D.	85	95
[67]	Werber et al. (2016)	5,844 mg/L NaCl	75	15/-	N.D.	B-value was used	100	100
[110]	Shi et al. (2017)	1000 mg/L NaCl	N.D.	N.D.	N.D.	100	N.D.	N.D.
[111]	Wei et al. (2017)	3000 ppm NaCl	60-98	15	8	100	100	100
[91]	Karabelas et al. (2018)	2,000 ppm	70	N.D.	N.D.	N.D.	85	95

Table 3. Models and considerations used for the simulations in each reference.

Reference	Author (Year)	Model					
		Variation in an element	Feed flow pressure loss	Permeate flow pressure loss	Feed side mass transfer coefficient	Osmotic pressure	Chronological change
[109]	Zhu et al. (2009)	Not considered	Not considered	Not considered	Not considered	25.3 bar (35,000 mg/L TDS)	Not considered
[66]	Cohen-Tanugi et al. (2014)	Considered in axial direction	Fanning friction factor $f=\mu^3(16d_F^2u_F^2\rho_F^2/\mu^2+0.4892(d_Fu_F\rho_F/\mu)^{2.964})/d_F^3u_F^3\rho_F^3$	Not considered	Correlation of Re $Sh=2.53(1.5Re^{2.78}+14.2Re^2)^{0.2363}$	van't Hoff equation $\Delta\pi=2C_FRTR_0exp(J/k)$	Not considered
[70]	Shrivastava et al. (2015)	N.D.	Darcy friction factor $f_D=aRe^b$	Darcy friction factor $f_D=aRe^b$	Correlation of Re and Sc $Sh=aRe^bSc^c$	OLI Analyzer 3.1	Not considered
[69]	McGovern et al. (2016)	Considered in axial direction	0	0	5.0×10^{-5} m/s (constant)	25.6bar (30,000 mg/L)	Not considered
[67]	Werber et al. (2016)	Considered in axial direction	0	0	2.77×10^{-5} m/s (constant)	van't Hoff equation $\Delta\pi=2C_FRTR_0exp(J/k)$ or OLI activity coefficient model	Not considered
[68]	Mazlan et al. (2016)	Considered in axial direction	Darcy friction factor $f_D=2.4\times6.23Re^{-0.3}$	0	4.0×10^{-5} m/s (constant)	van't Hoff equation $\Delta\pi=1.64X_MRT/v_M$	Not considered
[110]	Shi et al. (2017)	Considered in axial direction	Darcy friction factor $f_D=6.23Re^{-0.3}$	Darcy friction factor $f_D=105Re^{-0.8}$	Correlation of Re and Sc $Sh=0.065Re^{0.875}Sc^{0.25}$	N.D.	Not considered
[111]	Wei et al. (2017)	Considered in axial direction	Darcy friction factor $f_D=6.23Re^{-0.3}$	Not considered	Correlation of Re and Sc $Sh=aRe^bSc^c$	Pitzer equation	Not considered
[91]	Karabelas et al. (2018)	Considered in axial and circumferential direction	N.D.	Permeability coefficient 2.0×10^{-10} m^2	N.D.	N.D.	Not considered

Table 4. Results of relationship between membrane permeability (A value) and SEC in each reference for single-stage SWRO.

Author (Year)	Results	Reference
Zhu et al. (2009)	Permeability of high permeable membrane is near thermodynamic limit in single-stage RO. Having little economic incentive for higher permeable membranes in SWRO.	[109]
Cohen-Tanugi et al. (2014)	A-value: 1 to 3 LMH/bar ⇒ Feed pressure: 70 to 63 bar (SEC: 15% down) A-value > 3 LMH/bar has little effect on energy consumption.	[66]
Shrivastava et al. (2015)	A-value > 4.99 LMH/bar approaches to no effect on energy consumption.	[70]
McGovern et al. (2016)	Roughly 4-5 times of current A-value (1 to 2 LMH/bar) is the thermodynamic limit unless increasing mass transfer coefficient.	[69]
Werber et al. (2016)	A-value: 0.2 to 1.0 LMH/bar ⇒ SEC: 1.55 kWh/m^3 down (45%) A-value: 2 to 10 LMH/bar ⇒SEC: 0.06 kWh/m^3 down (3.7%) A-value: 10 to 100 LMH/bar ⇒SEC: 1.0% down When A-value is 2 LMH/bar, hydraulic pressure is only 7.6% above the brine osmotic pressure.	[67]
Mazlan et al. (2016)	A-value > 10 LMH/bar has almost negligible economic incentive.	[68]
Shi et al. (2017)	A-value > 3-5 LMH/bar has little impact unless improving mass transfer and decreasing pressure loss. A-value > 5 LMH/bar has negligible benefit for the process productivity.	[110]
Karabelas et al. (2018)	A-value accounts for roughly 24% of SEC.	[91]

Table 5. Results of relationship between permeability (A value) and SEC in each reference for single-stage BWRO.

Author (Year)	Results	Reference
Zhu et al. (2009)	There may be benefit in increasing A-value at low recovery, but associated cost, pretreatment, brine management are needed.	[109]
Cohen-Tanugi et al. (2014)	A-value: 1.5 to 4.5 LMH/bar ⇒ Feed pressure: 12 to 6.4 bar (SEC: 45% down) A-value > 5 LMH/bar has little effect on energy consumption.	[66]
Shrivastava et al. (2015)	Increasing A-value begins to approach the thermodynamic barrier.	[70]
Werber et al. (2016)	A-value: 4 to 10 LMH/bar ⇒ SEC: 2.2% down	[67]

assumed to be zero if the water permeate flux is lower than the critical flux.

Feed concentration was assumed to be 32,000 mg/L NaCl with a recovery rate of 40%. The mass transfer coefficient of salt at membrane surface on the feed side was calculated from a correlation. Osmotic pressure was calculated using a modified van't Hoff equation. Three different membrane water permeabilities of 1.04, 1.40 and 2.19 LMH/bar were used for the simulation.

Fig. 9 shows calculated results for the specific energy consumption against operating time. The specific energy consumption increased between 0.3-0.6 kWh/m^3 in 60 days. The membrane with 2.19 LMH/bar water permeability had the lowest specific energy consumption at first. However, rate of increase of the specific energy consumption during operation was higher than for other two membranes, and this membrane had the highest specific energy consumption by 90 days of operation. This is because operation with higher permeate water flux brings more foulants to the membrane surface. This in turn increases the resistance to permeation and requires an increase of feed pressure to maintain the set flux.

Although the authors compared how the membrane water permeability affects the chronological change of the specific energy consumption, the relationship between tolerance to membrane fouling and specific energy consumption was not included.

As mentioned in 3.1.1.1, no references have calculated the relationship between membrane performance and specific energy consumption while including the effect of fouling or ageing over time. These effects varying the RO membrane element performance, and thus the specific energy consumption varies over time. Therefore, chronological effects should be considered in any prediction of the

relationship between RO membrane element performance and RO plant cost.

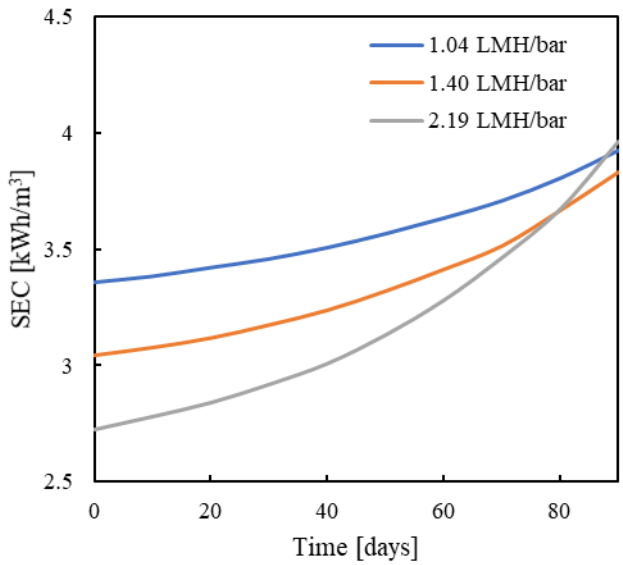

Fig. 9 Calculated specific energy consumption as a function of operating time for conventional single-stage SWRO with three membrane water permeabilities, extracted from [130].

3.1.1.3 Salt permeability

The salt permeability of a membrane also has an effect on the specific energy consumption. If the salt in feed water is completely rejected by membrane, the brine concentration depends only on recovery rate. However, in an actual RO membrane, salt rejection rate is not 100%, and the concentration of the brine becomes lower than when a perfect membrane is used. In a conventional single-stage RO process, the specific energy consumption at a thermodynamic limit is expressed by the following equation:

$$SEC = \frac{\left(1 - \eta_E(1 - RR)\right)R_0}{\eta_p RR(1 - RR)}\pi_F \tag{14}$$

where η_E is the efficiency of the ERD, η_p is the efficiency of the feed pump, and R_0 is the rejection rate of the RO system [71, 109, 114, 115]. Higher membrane rejection brings higher specific energy consumption, while lower membrane rejection brings lower specific energy consumption. In terms of decreasing specific energy consumption, membrane rejection should be lower. Obviously, however, the permeate salinity must satisfy the specific need for final water quality at the RO plant.

If the overall desired rejection is not accomplished by a single-stage system, a permeate two-pass process is a feasible approach. The specific energy consumption of the permeate two-pass RO can be obtained by following equation:

$$SEC = \frac{R_{0,max}}{RR_2 - RR_t} + \frac{R_{0,t} - R_{0,max}}{1 - RR_2} \tag{15}$$

where $R_{0,max}$ is the available highest membrane rejection, RR_2 is the recovery rate of second pass, RR_t is the recovery rate in the total system, and $R_{0,t}$ is the total rejection of the system.

For a permeate two-pass RO process, Zhu et al. [114] calculated the effect of RO membrane rejection to minimize the energy consumption. The relationship between available highest membrane rejection and nominal specific energy consumption in permeate two-pass RO is shown in Fig.10. The pump efficiency was assumed to be 100%, and the target recovery rate and salt rejection of the system taken to be 50% and 99%, respectively.

As can be seen from Fig. 10, the higher the membrane rejection, the higher reduction of specific energy consumption that can be obtained in permeate two-pass RO process. If the desired overall salt rejection can be achieved in a single-pass, then a single-pass configuration will be more energetically favorable than a two-pass configuration for the same total water recovery rate and salt rejection.

On the other hand, Park et al. [131] calculated the effect of membrane boron rejection rate on the specific energy consumption considering the effect of fouling for permeate two-pass SWRO. The configuration used six SWRO elements in the first pass and four BWRO elements in the second pass.

Three boron rejection rates of 88%, 90%, and 92% were assumed for SWRO elements for fixed water permeability. In addition, the boron rejection rate for the BWRO elements was 55%, and the target boron rejection of the plant was 85%. To consider the effect of fouling, the mass transfer coefficient was assumed to be 63.1% of the original value as the result of fouling.

As the boron rejection of the SWRO elements increased from 88 to 90 and 92%, the specific energy consumption decreased from 4.91 to 4.03, to 3.54 kWh/m^3. It was concluded

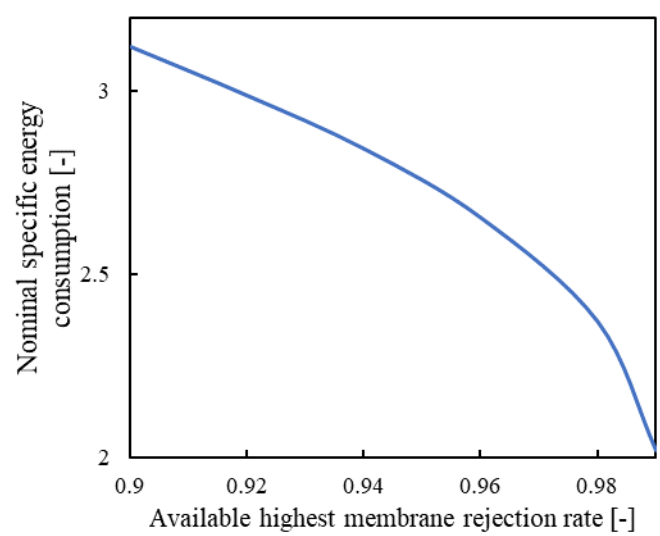

Fig. 10 Calculated nominal specific energy consumption as a function of available highest membrane rejection for two-pass SWRO process, extracted from [114].

that, as for SWRO, decreasing boron permeability can be an effective method for reducing specific energy consumption depending on conditions of plant construction, regulations for permeate water quality, and feed water quality.

3.1.2 RO element performance

3.1.2.1 Feed side pressure loss

A pressure loss in feed side path decreases effective transmembrane pressure, as shown in equation (2). If the feed side pressure loss decreases, the feed pump pressure can be decreased. For industrial application of RO elements, several elements are connected in series in a module, and the feed side pressure loss should be calculated per module.

Many studies [11, 132-137] have been conducted to decrease the feed side pressure loss by improving feed spacer configuration. Although no references directly estimated and showed relationship between feed-side pressure loss and the specific energy consumption, some papers have evaluated the contribution of the feed-side pressure loss to the total specific energy consumption. It can be estimated how the feed-side pressure loss affects the system performance based on the contribution of the feed-side pressure loss to the total specific energy consumption. That is, if the feed-side pressure loss contributes 10% of the specific energy consumption, decreasing feed-side pressure loss by half can reduce the specific energy consumption by 5%.

Shrivastava et al. [70] calculated how a feed side pressure loss contributes to the specific energy consumption of an RO plant. For SWRO, they found that the feed side pressure loss accounts for 1.3% of the specific energy consumption. On the other hand, for BWRO, the feed side pressure loss accounts for 11.9% of the specific energy consumption. The simulation conditions were shown in Table 1 for SWRO and Table 2 for BWRO.

Karabelas et al. [91] also calculated how a feed side pressure loss contributes to the specific energy consumption of an RO plant. For SWRO, they found that the feed side pressure loss accounts for 2.4% of energy loss in RO process. On the other hand, for BWRO, the feed side pressure loss accounted for 9.5% of the energy loss in RO. These values were a little different from the values found by Shrivastava et al. [70], perhaps due to differences of conditions and models used for simulations, as shown in Tables 1-3. In particular, the feed concentrations were quite different for SWRO.

In summary, although decreasing feed-side pressure loss by improving feed spacer configuration can decrease the specific energy consumption, its effect is only slight (likely less than 1%) for SWRO, whereas it can be more significant for BWRO. This is because the feed-side pressure loss is smaller than the effective transmembrane pressure by an order of magnitude. As the effective transmembrane pressure decreases with variation of the feed salinity, recovery rate, and so on, the feed-side pressure can contribute more to the specific energy consumption.

3.1.2.2 Permeate side pressure loss

A pressure loss in the permeate-side path decreases effective transmembrane pressure as shown in equation (2). However, as shown in Table 3, the permeate side pressure loss was not taken into consideration in some references, since it is negligible compared to applied pressure.

Although no references have directly estimated the relationship between permeate side pressure loss and the specific energy consumption, some papers evaluated the contribution of the permeate-side pressure loss to the total specific energy consumption. It can be estimated how the permeate-side pressure loss affects the system performance based on the contribution of the permeate-side pressure loss to the total specific energy consumption. That is, if the permeate-side pressure loss contributes 10% of the specific energy consumption, decreasing permeate-side pressure loss by half can reduce the specific energy consumption by 5%.

Shrivastava et al. [70] calculated how a permeate side pressure loss contributes to the specific energy consumption in an RO plant. For SWRO, the permeate side pressure loss accounts for 2.4% of the specific energy consumption. On the other hand, for BWRO, the permeate side pressure loss accounts for 8.4% of the specific energy consumption. The simulation conditions were shown in Table 1 for SWRO and Table 2 for BWRO.

Karabelas et al. [91] also calculated how a permeate side pressure loss contributes to the specific energy consumption RO. For SWRO, permeate side pressure loss accounts for 0.1% of energy consumption in the RO process. On the other hand, for BWRO, permeate side pressure loss accounts for 0.4% of the energy loss in the RO process. As seen for the feed side loss, these values were considerably different from the values found by Shrivastava et al. [70]. The conditions and models used for these simulations are shown in Tables 1-3. The significant difference between [91] and [70] was the model used to calculate permeate side pressure loss. Karabelas et al. [91] used the experimentally evaluated permeability of permeate spacer, while Shrivastava et al. [70] used the Darcy-Weisbach equation.

Shi et al. [110] reported that the permeate side pressure loss is likely to become a very significant consideration as the membrane water permeability increases. When the membrane water permeability exceeds a critical value, the permeate side pressure loss limits the system permeability and limits the benefit of increasing the membrane water permeability.

In summary, the effect of decreasing the permeate side pressure loss is small because the permeate-side pressure loss is smaller than the effective transmembrane pressure by one order of magnitude; but as the effective transmembrane pressure decreases with variation of the feed salinity, recovery rate, etc., the permeate-side pressure can contribute more to the specific energy consumption. As the water permeate flux of the system increases, the permeate-side pressure loss can become a significant factor; however, increasing average water flux of a system also increases the risk of fouling. Therefore, simulation of these effects should consider the influence of an increasing fouling rate.

On the other hand, Al-Obaidi et al. [138] evaluated the impact of membrane length (the length perpendicular to the axial direction) on the specific energy consumption for RO process to remove chlorophenol from wastewater with membrane surface area fixed. The membrane surface area of the element was fixed at 7.845 m^2 with a diameter of 4 inches. The membrane length is related to permeate side pressure loss, and if membrane length is short, the flow path becomes shorter and permeate side pressure loss decreases [139]. The results of evaluation for cases with and without an ERD are shown in Fig. 11. Increasing membrane width, which means decreasing membrane length at the same time, decreased the specific energy consumption as a result of the reduction of permeate side pressure loss.

The effect of membrane length can be valuable depending on the geometry of RO elements and operating conditions, but it is also necessary for manufacturers to consider the productivity of RO elements.

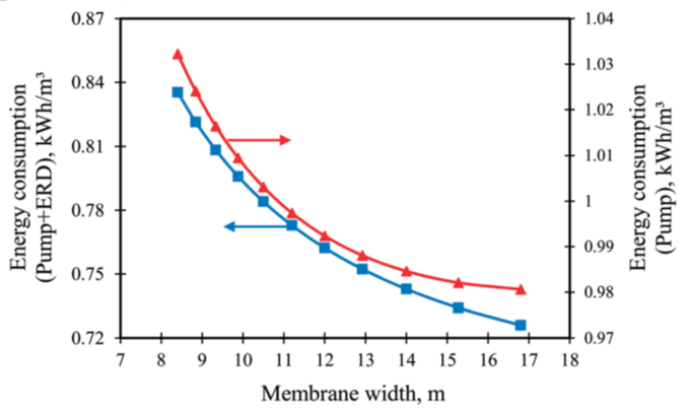

Fig. 11 Calculated specific energy consumption as a function of membrane width with and without ERD for waste water RO treatment, reprinted from [138].

3.1.2.3 Feed side mass transfer coefficient

The mass transfer coefficient of salt on the feed side of the membrane controls the degree of concentration polarization. A higher feed-side mass transfer coefficient can reduce concentration polarization and can reduce the feed pump pressure required to obtain a given amount of permeate flow. The mass transfer coefficient is determined by the feed spacer configuration, the element design, system configuration, operating conditions, and the system conditions. Many studies have attempted to increase the mass transfer coefficient by improving feed spacer configuration [11, 88, 132, 135-137, 140-145]. In addition, some papers report other methods to improve the mass transfer coefficient by introducing an external force such as gas sparging, vibration, or electro-osmosis [146-148].

Shrivastava et al. [70] calculated how much concentration polarization contributes to the specific energy consumption in an RO plant. For SWRO, concentration polarization accounts for 6.3% of the specific energy consumption. On the other hand, for BWRO, the concentration polarization accounts for only 1.76% of the specific energy consumption. The simulation conditions were shown in Table 1 for SWRO and Table 2 for BWRO.

Karabelas et al. [91] also calculated how concentration polarization contributes to the specific energy consumption in an RO plant. For SWRO, they found that concentration polarization accounts for 2.4% of the specific energy consumption. On the other hand, for BWRO, concentration polarization accounts for 1.3%. The difference from the values from Shrivastava et al. [70] may be due to differences in the model for the mass transfer coefficient and osmotic pressure, and the simulated conditions, which are shown in Tables 1-3.

Shi et al. [110] reported how concentration polarization affects the RO membrane water permeability from experiments using cross-flow cells. They reported that if the mass transfer coefficient is within the range of 1.0×10^{-5} and 1.0×10^{-4} m/s (the usual range of an RO system), concentration polarization limits the increase of system permeability. As membrane water permeability increases, the system permeability reaches a plateau at a certain value, once reaching a plateau, further increases of membrane water permeability will not have the effect of increasing the system permeability. The same conclusion had been reported previously by McGovern and Lienhard [69], as described in Section 3.1.1.1.

In summary, the mass transfer coefficient can contribute more than 1% of the specific energy consumption for both SWRO and BWRO, but its effect is larger for SWRO than for BWRO. Therefore, increasing the feed side mass transfer coefficient is more important for SWRO than for BWRO. Furthermore, although it is thought that as recovery ratio increases, the concentration polarization increases, and the importance of raising the mass transfer coefficient further increases, no literature appears to have discussed the issue.

3.1.2.4 Fouling to the feed spacer

As mentioned in 3.1.1, water permeate flux varies during operation due to fouling. Fouling occurs not only on the membrane surface but also on the feed spacer. Attachment of foulants on feed spacer increases the feed side pressure loss, and thus the effective transmembrane pressure decreases. It increases the feed pump pressure needed to produce the same amount of permeate water flow rate. No literature has directly studied the relationship between fouling of the feed spacer and the specific energy consumption of RO, but many studies have been conducted to improve the anti-fouling propensity of the feed spacer [11, 149-160].

Bates et al. [151, 152] measured the transition of feed side pressure loss for a variety of elements using three different feed spacers. Operation was done over three periods. At first, a spacer of 28 mil (0.71 mm) thickness was used, secondly a spacer of 31 mil (0.79 mm) thickness with a different geometry was used, and finally a spacer of 34 mil (0.86 mm) thickness with different geometry was used. The element with spacers of 28 mil thickness required clean-in-place (CIP) events 5 times in 250 days to maintain the acceptable pressure loss in the vessel, but the element with spacers of 31 mil

thickness needed CIP only once, and the element with spacers of 34 mil thickness did not need CIP at all.

The result showed that increasing anti-fouling propensity of the feed spacer suppressed the increase of feed side pressure loss over time, and consequently it was possible to suppress the increase of specific energy consumption over time.

3.1.2.5 Membrane surface area

Al-Obaidi et al. [138] evaluated the impact of membrane surface area on the specific energy consumption of an RO process to remove chlorophenol from wastewater in cases with and without an ERD. They modeled a 50% increase of membrane surface area from 7.845 m^2 to 11.768 m^2 by increasing either membrane length or width. The simulation assumed a 4-inch size membrane element, 800 mg/L of chlorophenol in the feed, and a feed flow rate 22.3 m^3/d.

In case without ERD, increasing membrane length decreased the specific energy consumption by 23.6% from 1.03 to 0.78 kWh/m^3, while increasing membrane width decreased the specific energy consumption by 28.4% from 1.03 to 0.73 kWh/m^3. On the other hand, in case with ERD, increasing membrane length decreased the specific energy consumption by 15.7% from 0.83 to 0.70 kWh/m^3, while increasing membrane width decreased the specific energy consumption by 24.1% from 0.83 to 0.63 kWh/m^3. These findings are shown in Fig. 12.

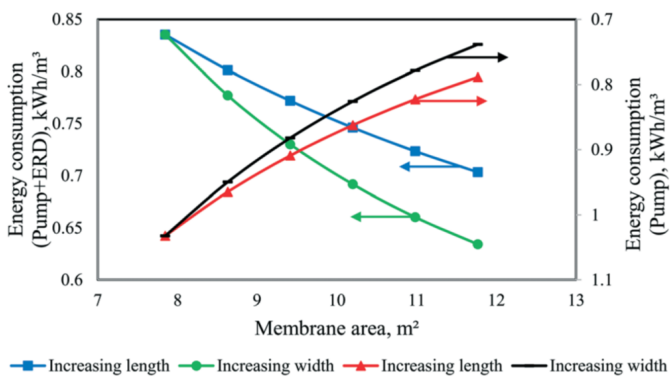

Fig. 12 Calculated specific energy consumption as a function of membrane area when with and without ERD for wastewater treatment RO process, reprinted from [138].

In addition, increasing membrane surface area by concurrently increasing both membrane length and membrane width with a fixed RO module volume decreased the specific energy consumption by 21.0% with the ERD and by 26.7% without the ERD, as shown in Fig. 13.

While the effect of membrane surface area can be valuable depending on the geometry of RO elements and operating conditions, it is also necessary to consider the productivity of RO elements.

Gu et al. [76] predicted the effect of the number of membrane leaves on specific energy consumption by using both a plate-like model and a spiral model. They assumed a total membrane surface area of 4.5 m^2, and varied the width of membrane leaves from 4.5 m (1 leaf) to 0.45 m (10 leaves). In addition, they also varied the length of membrane leaves from 3 m (1 leaf) to 0.3 m (10 leaves). As the width of a membrane leaf decreases, the permeate side pressure loss decreases. On the other hand, as the length of a membrane leaf decreases, the feed side pressure loss decreases.

As a result of the simulation, the permeate flow decreases as the number of leaves increase because the effective membrane area becomes smaller due to the presence of the glue line. In addition, the specific energy consumption is maximized when the number of leaves is two for varying membrane leaf width, and at three leaves for varying membrane lead length for the case of a spiral model.

Increasing membrane surface area can increase the permeate flow rate so that the specific energy consumption can be decreased, but at the same time, increasing membrane surface area increases the cost of an RO element. Therefore, increasing membrane surface area to reduce energy consumption (i.e., OPEX) can result in an increase of CAPEX.

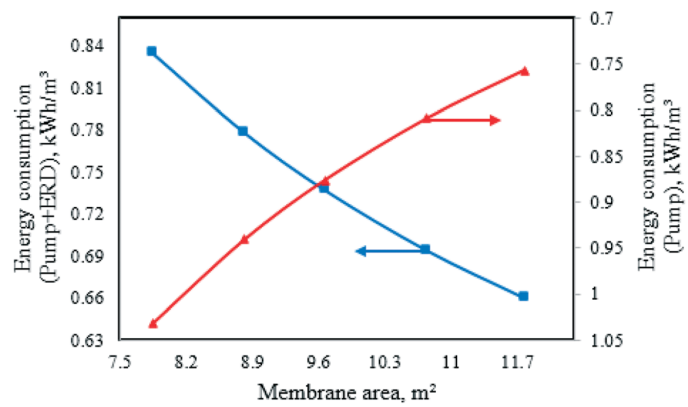

Fig. 13 Calculated specific energy consumption as a function of membrane area increased by extending both membrane length and membrane width simultaneously with and without ERD for wastewater treatment RO process, reprinted from [138].

3.2 Costs other than energy

3.2.1 RO membrane performance

The RO membrane element performance is also related to costs of an RO plant other than energy. Although no literature has directly evaluated the relationship between RO membrane element performance and RO plant cost, some literature has indirectly studied the influence of RO membrane element performance on RO plant cost.

Increasing membrane water permeability offers the possibility of not only decreasing feed pump pressure but also decreasing membrane area. Decreasing membrane area means using fewer RO elements and modules.

There are four options to reduce the process cost by applying RO membrane elements with higher water permeability for conventional single-stage RO. The first is to reduce the feed pump pressure while keeping permeate flow rate as mentioned in 3.1.1.1. The second is to increase the recovery rate. Although increasing recovery rate results in an increase in osmotic pressure in feed side path, RO elements

with higher permeability have the potential to maintain the same permeate flow rate even if the recovery rate increases. The third is to increase permeate flow rate. Operating while keeping feed pump pressure and recovery rate increases the permeate flow rate and feed flow rate at the same time. The fourth is to decrease the membrane area while keeping the same permeate flow rate [105].

Busch et al. [105] assessed the CAPEX and OPEX reductions with higher permeable SWRO elements. They compared the energy use, power cost, water cost by replacing SW30HR-380 with 28.4 m^3/d of permeate flow rate and 99.75% of NaCl rejection rate by SW30HR LE-400 with 34.1 m^3/d of permeate flow rate and 99.70% of NaCl rejection rate using the test results for each element. Test conditions and calculation assumptions were 32,000 mg/L NaCl of feed concentration, 8% of recovery rate, 55 bar of feed pump pressure, 5 years of operating time, 20% of RO membrane elements replacement rate per year, 90% of pump efficiency, and 0.08 US$/kWh of power cost. The pretreatment, chemical cleaning, and other costs were not considered. They indicated that decreasing membrane area by using higher water permeability RO elements can decrease the water cost by 4.7% from 0.190 to 0.181 US $/$m^3$ with the same energy cost.

Zhu et al. [109] assessed the specific membrane cost relative to the specific energy cost by converting the membrane price into energy units. For a single-stage RO process, the specific membrane cost was obtained by the following equation:

$$SMC = \frac{m_A \beta}{\varepsilon} \times \frac{A_m}{Q_P} = \frac{m_A \beta}{\varepsilon Q_P}\left(\frac{Q_P}{A(\Delta P - \overline{\Delta\pi})}\right) \tag{16}$$

where β and ε are conversion factors, m_A is the membrane unit price, A_m is the membrane surface area, ΔP is the transmembrane pressure and $\overline{\Delta\pi}$ is the average osmotic pressure in the feed side. In the thermodynamic limit, the transmembrane pressure and the average osmotic pressure in the feed side are related by the following equations:

$$\Delta P = \frac{\pi_F R_0}{1 - RR} \tag{17}$$

$$\overline{\Delta\pi} = \frac{\pi_F R_0 \ln\left(\frac{1}{1 - RR}\right)}{RR} \tag{18}$$

Thus, the normalized specific membrane cost at the thermodynamic limit is obtained by the following equation:

$$SMC_{min}^{norm} = \frac{m_A \beta}{\varepsilon A R_0 \pi_F^2 \left[\frac{1}{1 - RR} - \frac{1}{RR}\ln\left(\frac{1}{1 - RR}\right)\right]} \tag{19}$$

On the other hand, the normalized specific energy consumption which can be obtained by dividing equation (14) by π_F was expressed by the following equation:

$$SEC_{min}^{norm} = \frac{\left(1 - \eta_E(1 - RR)\right)R_0}{\eta_p RR(1 - RR)} \tag{20}$$

Therefore, the specific membrane cost relative to the specific energy consumption (MER) was expressed by introducing the dimensionless factor R_{MEC} in the following equations:

$$MER = \frac{SMC_{min}^{norm}}{SEC_{min}^{norm}} = \frac{R_{MEC}\eta_p RR(1 - RR)}{\left(\frac{1}{1 - RR} - \frac{1}{RR}\ln\left(\frac{1}{1 - RR}\right)\right) \times \left(1 - \eta_E(1 - RR)\right)} \tag{21}$$

$$R_{MEC} = \frac{\beta m_A}{\varepsilon A (R\pi_0)^2} \tag{22}$$

The R_{MEC} reflects the impact of feed water osmotic pressure, salt rejection, membrane permeability, and the price of electrical energy and the membrane module on the MER ratio. In general, R_{MEC} ranges from ~0.001 to 1; it is 0.01 for seawater of ~35,000 mg/L TDS and 1 for brackish water of 1000 mg/L TDS. Assuming typical values for each parameter in equation (21) and (22), when the parameter R_{MEC} is 0.01, the MER value is within the range of 3-12%. For SWRO, the energy cost contributes 40-50% of the total water production cost; therefore, the ratio of the specific membrane cost to the total water production cost is about 1.2-6%. Hence, doubling the membrane water permeability halves the specific membrane cost so that the total water production cost is reduced to 0.6-3%. When the cost of pressure vessels is taken into consideration, the decrease of total water production cost is 0.7-3.5%.

Cohen-Tanugi et al. [66] calculated the total number of pressure vessels needed for a 100,000 m^3/d permeate as a function of membrane water permeability for single-stage SWRO with 42,000 ppm of feed salinity and single-stage BWRO with 2,000 ppm of feed salinity assuming fixed feed pump pressure. The results of calculation are shown in Fig. 14. Tripling membrane water permeability would allow SWRO plants to produce the same amount of permeate with 55% fewer pressure vessels. However, more energy is needed due to higher velocity in feed side path which increases the pressure loss, thus eventually, the specific energy consumption would also increase by 6%.

On the other hand, Mazlan et al. [68] showed the relationship between membrane water permeability and specific membrane surface area for SWRO, although the cost was not discussed directly. The simulation conditions are shown in Table 1, and the models used are shown in Table 3. As mentioned in 3.1.1.1, as membrane water permeability increases, the effect of reducing specific energy consumption approaches an asymptote. However, for membrane surface area, although the effect of decreasing membrane surface area by increasing membrane water permeability is diminished as the membrane water permeability increases, it has an ongoing effect even if membrane water permeability exceeds 3 LMH/bar until 100 LMH/bar as shown in Fig. 15. This

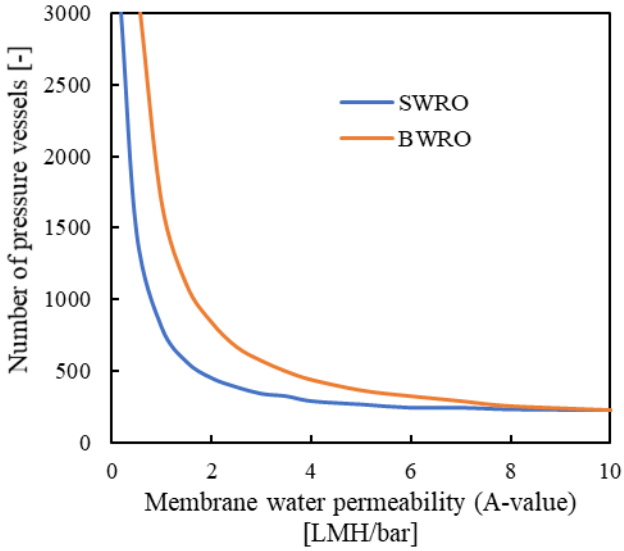

Fig. 14 Calculated required number of pressure vessels as a function of membrane water permeability for single-stage SWRO with 42,000 ppm feed, 42% recovery rate, 70 bar feed pump pressure and single-stage BWRO with 2,000 ppm feed, 65% recovery rate, and 12 bar feed pump pressure for total capacity of 100,000 m^3/d, extracted from [66].

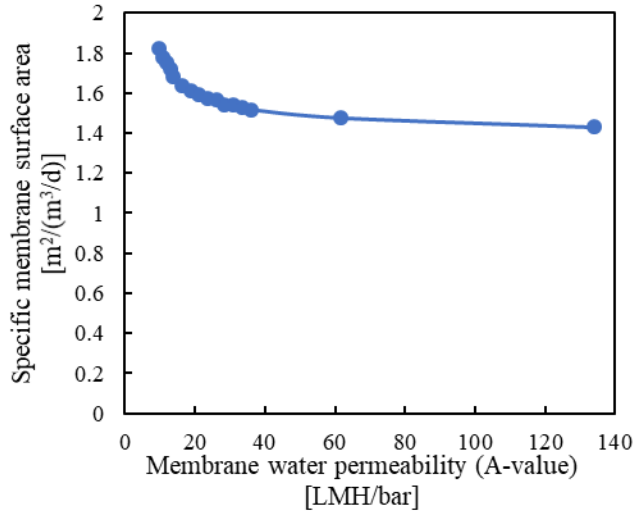

Fig. 15 Calculated specific membrane area as a function of membrane water permeability for single-stage SWRO with 35,000 mg/L and 50% recovery rate, extracted from [68].

behavior is in contrast with the rapidly flattening energy consumption curve shown in Fig. 7.

References [66] and [68] showed large differences about how membrane area can be reduced by increasing membrane water permeability. In reference [66], the number of pressure vessels, which is proportional to membrane surface area, is approaching an asymptote at membrane water permeability over 5 LMH/bar for SWRO. In reference [68], the membrane surface area can be decreased even past 10 LMH/bar. This difference may be due to the difference of models and conditions used for the simulations: the models for friction factor for feed side pressure loss, osmotic pressure, and the mass transfer coefficient were different. In reference [68], the mass transfer coefficient is constant at any position inside the element. In the region of membrane water permeability over 5 LMH/bar, the effect of pressure loss and mass transfer coefficient can be much larger, and as a result the difference of the model assumptions might cause the large difference in trends for membrane area.

Note that decreasing membrane area results in higher flux operation, thus increasing the risk of fouling and the frequency of chemical cleaning or RO element replacement, both resulting in an increase in cost. Therefore, to estimate how increasing membrane water permeability affects the cost of an RO plant, the effect of fouling should be included in the simulation.

3.2.2 RO element performance and other cost drivers

Franks et al. [118] reported the difference of chemical cleaning cost when conventional RO membrane elements were replaced by elements which have higher permeability and thicker feed spacers. The test was conducted for a single-stage process in BWRO with 1500 mg/L feed NaCl, seven elements per module, 55% of total recovery rate, and 25.2 LMH of system average water flux. As a result, replacement of the elements decreased the frequency of chemical cleaning from twice a year to once a year. Therefore, the annual cleaning cost was estimated to decrease from 180,000 to 90,000 US$/year.

Malek et al. [161] and Pervov et al. [162] evaluated the relationship between process cost and recovery rate. Although the influence of RO membrane element performance on the cost was not mentioned, it was indicated that as the recovery rate increases CAPEX increases while OPEX decreases. Therefore, there exists an optimum point of recovery rate to minimize the cost.

Ruiz-Garcia et al. [163] compared the difference of cost between when the specific energy consumption increases due to chronological effects such as fouling with and without replacing the RO membrane elements from 80,000 hours operation. The costs of electrical energy, chemical cleaning and membrane replacement were considered. The best choice was found to be not replacing the RO membrane elements for at least the first 80,000 hours. Therefore, if the tolerance to the chronological change of RO membrane element increases, it can be thought that the performance can be more cost effective.

Vanoppen et al. [164] calculated the influence of pre-treatment to reduce the cost of brine discharge. By introducing ion-exchange as pre-treatment, brine discharge cost was reduced because of increasing recovery rate, thus the total cost was reduced from 1.9 to 1.6 €/m^3. This indicates increasing recovery rate decreases the total cost if an RO membrane element withstands high recovery operation.

Sethi et al. [165] and Suarez et al. [166] gave models to calculate CAPEX drivers such as pumps, pipes, valves, instruments, controls, tanks, frames, miscellaneous items, and membranes, although the effect of RO membrane element performance was not included in the models. Suarez et al. [166] showed models to calculate OPEX in addition to the

models of CAPEX. All the costs above other than the pump are a function of membrane surface area. The costs of piping and valves are functions of the 0.42th power of membrane area, instruments and controls are functions of the 0.66th power of membrane area, tanks and frames are functions of 0.53th power of membrane area, and miscellaneous costs are a function of 0.57th power of membrane area. In addition, membrane cost is proportional to the membrane area.

4. Closed-circuit RO

4.1 Outline of Closed-circuit RO

Closed-circuit reverse osmosis (CCRO) is a semi-batch process which includes circulation of brine water. The circulated brine is mixed with pressurized raw water, then the mixture is provided to the RO membrane modules again. The raw water is continuously added to the system over time, and once reaching the desired recovery rate, then the concentrated brine is discharged outside the system and replaced by new raw water for the next cycle as shown in Fig.16.

Several designs have been proposed for CCRO [167-172]. The CCRO process uses shorter modules which include smaller numbers of RO elements compared with conventional modules. Two operational modes, PFD (plug flow desalination) and CCD (closed-circuit desalination), are applied sequentially under fixed flow rate with variable pressure conditions.

As for a conventional continuous RO system, the feed pump pressure must be higher than the maximum osmotic pressure in the feed side path. However, in the CCRO process, as osmotic pressure in the feed side path increases, the feed pump increases over time, thus it reduces the specific energy consumption for CCRO relative to conventional continuous RO.

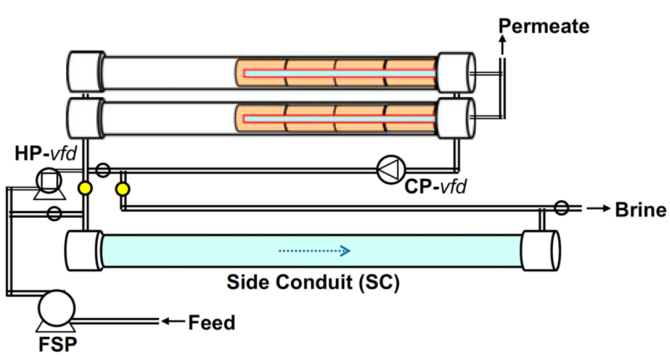

Fig. 16 Configuration of closed-circuit RO process, reprinted from [167].

4.2 Energy and cost

Although no literature has directly studied the relationship between RO membrane element performance and cost or energy consumption of the CCRO process, several references indicate the possibility of reducing the specific energy consumption and easier maintenance compared with conventional RO.

According to reference [167], which calculated the specific energy consumption of CCRO compared with conventional RO, CCRO can decrease the specific energy consumption by about 30% compared to conventional RO from 1.94 to 1.63 kWh/m^3 under the conditions of 35,000 ppm feed water concentration, 13 LMH average permeate water flux, and 50% recovery rate (Fig. 17).

In addition, according to reference [168], CCRO has potential to reduce fouling and scaling as a result of the design aspect of short modules and the operational aspect of PFD and CCD. Fouling may be prevented by frequent fast flush flow of fresh feed water. As for bio-fouling, in addition to the flush flow operation, the faster cross flow velocity due to short modules and large salinity variations of feed can reduce or eliminate the likelihood of bio-fouling. Scaling in conventional RO is normally associated with tail elements where brine concentration is high and cross flow velocity is low. In CCRO, low scaling characteristics are seen due to following four reasons: (1) the concentrate is recycled and diluted with fresh water at inlet of module and this dilution effect inhibits the formation of crystallized seeds; (2) a smaller number of elements per module can maintain a faster cross flow; (3) the cross-flow velocity and recovery rate for CCRO are fully controlled by operational set points, which can be changed online; and (4) the selection of an appropriate anti-scalant for a specific feed solute by using computer analysis programs of anti-scalant producers.

Efraty et al. [171] showed that CCRO process worked well in the Mediterranean Sea with much higher flux: 22 LMH, which is 40% higher than conventional SWRO.

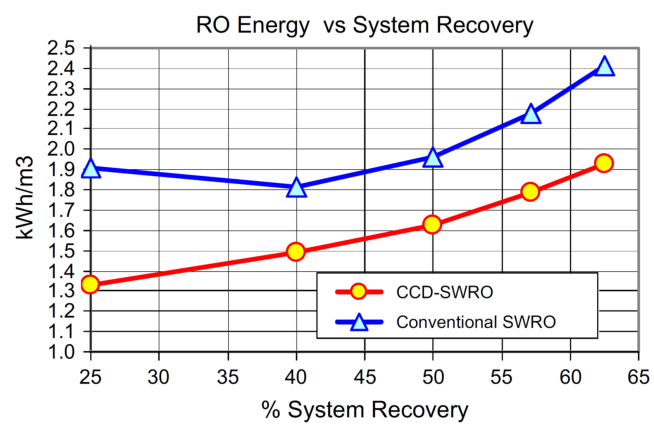

Fig. 17 Calculated specific energy consumption as a function of system recovery rate for SWRO in CCRO and conventional RO process, reprinted from [167].

5. Batch RO

5.1 Overview of Batch RO

Batch RO (BRO) is a fully batch process which can minimize the entropy generation due to mixing of raw water with circulated brine in CCRO process [69, 94, 173-181]. In BRO process, feed water is supplied only at the beginning of a cycle. It is circulated and concentrated over time, and once reaching the desired recovery ratio, the concentrated brine is discharged outside the system and replaced by new raw water for the next cycle. In one implementation (shown in Fig. 18), a variable-volume, pressurized tank stores brine to be

circulated. The tank must vary in volume to accommodate permeate leaving the system. Figure 13 shows an alternative implementation that uses only existing components including a tank at atmospheric pressure and a pressure exchanger. Part of the feed passes through the high-pressure pump to maintain same flow rates through the pressure exchanger [179].

5.2 Energy and cost

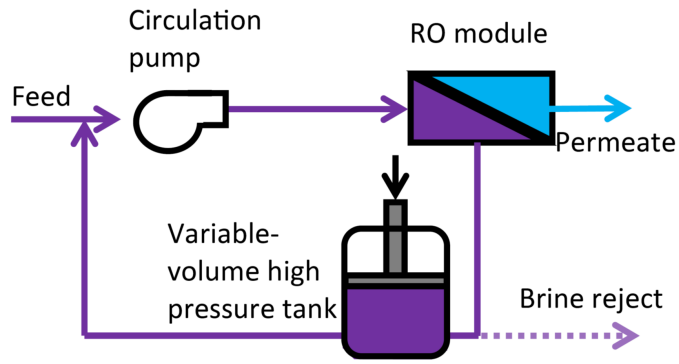

Fig. 18 Configuration of batch RO process reprinted from [179].

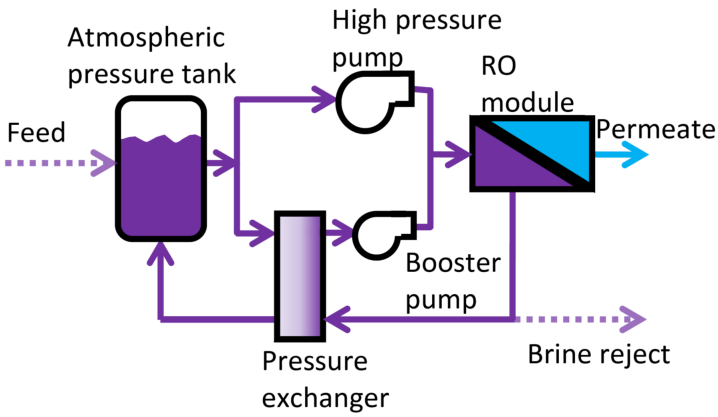

Fig. 19 Another configuration of batch RO process reprinted from [179].

5.2.1 Membrane water permeability

Warsinger et al. [178] evaluated the effect of membrane water permeability on the specific energy consumption in BRO. The specific energy consumption in BRO as a function of membrane water permeability for seawater and brackish water was shown in Fig. 20. For seawater, most of the energy savings (~13%) from higher permeable membranes are achieved by having up to 4 LMH/bar permeability, while for brackish water, energy savings (37%) does not diminish until about 7 LMH/bar. At these permeability values, increasing membrane water permeability by 10% results in less than 2% of benefit in energy savings. For low permeable (1 LMH/bar) membranes in seawater batch RO (SWBRO), the specific energy consumption is 1.94 kWh/m^3, while for high permeable (10 LMH/bar) membranes, the specific energy consumption is decreased to 1.63 kWh/m^3.

In this simulation, the feed concentration for seawater was 35,000 ppm, and 50% recovery rate. On the other hand, the feed concentration of brackish water was 5,000 ppm, and 66% recovery rate. In addition, the pump efficiency was 80%, average membrane water flux was 14.5 LMH, and the mass transfer coefficient was assumed to be a constant value of 2×10^{-5} m/s.

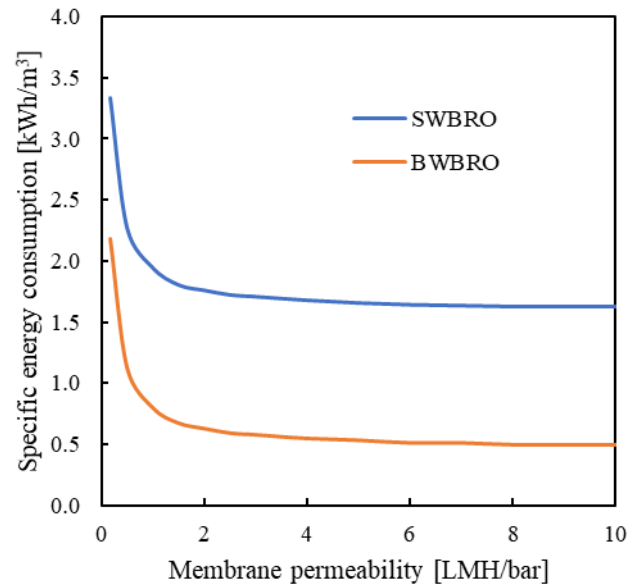

Fig. 20 Calculated specific energy consumption as a function of membrane water permeability for seawater BRO and brackish water BRO, extracted from [178].

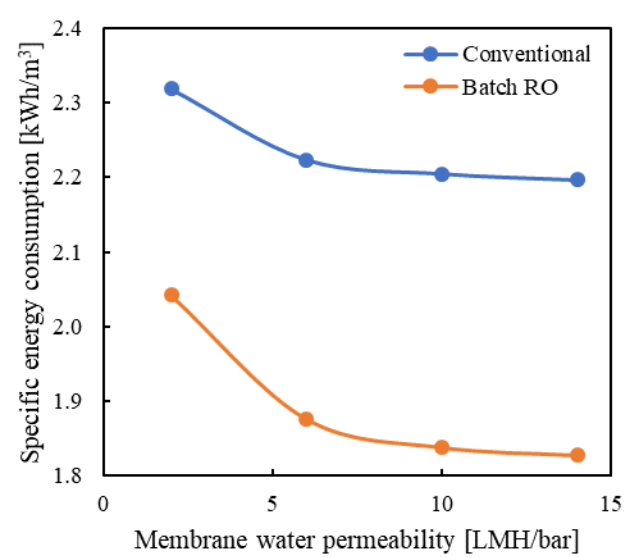

Fig. 21 Calculated specific energy consumption as a function of membrane water permeability for seawater BRO and conventional RO process, extracted from [177].

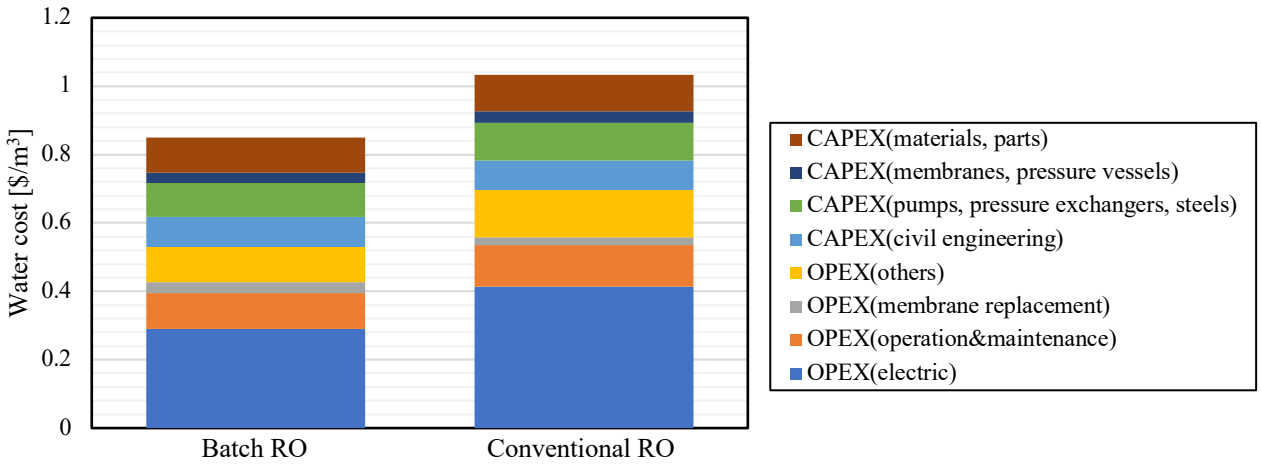

Fig. 22 Breakdown of water costs in BRO and conventional single-stage RO for a 4,000 m^3/d system of seawater desalination, extracted from [178].

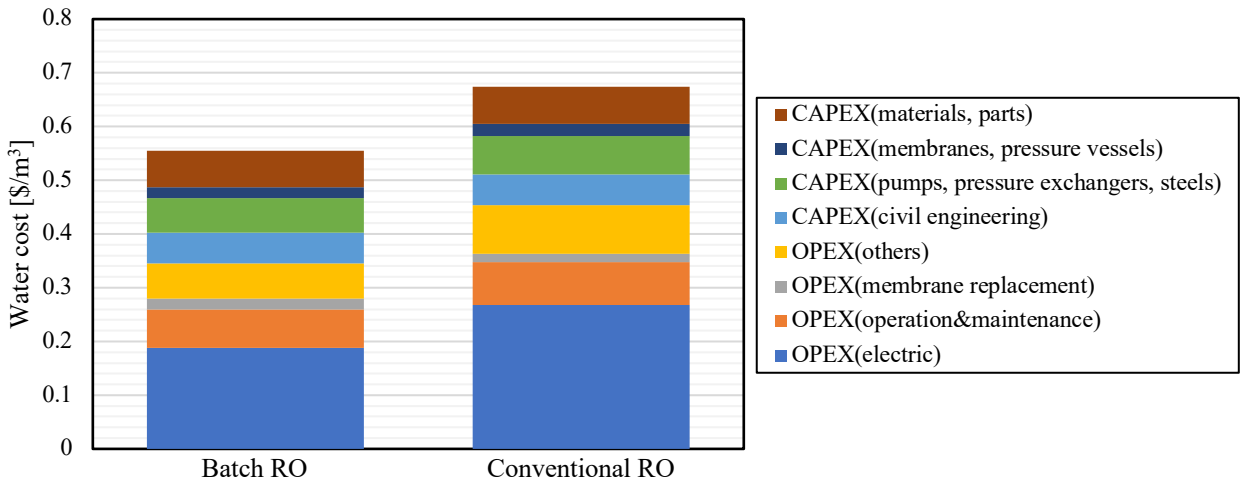

Fig. 23 Breakdown of water costs in BRO and conventional single-stage RO for a 10,000 m^3/d system of seawater desalination, extracted from [178].

In reference [177], Swaminathan et al. also showed the effect of increasing membrane water permeability on the specific energy consumption for SWBRO compared to conventional SWRO (Fig. 21). The specific energy consumption drops by about 10% (0.2 kWh/m^3) with an increase of membrane water permeability from 2 to 10 LMH/bar. On the other hand, for conventional RO, the specific energy consumption decreases by about only 0.11 kWh/m^3.

5.2.2 Cost

Warsinger et al. [178] evaluated the cost of BRO in the cases of conventional RO, batch RO, batch RO with ultra-permeable membrane for seawater desalination. The plant size was assumed as 4,000 m^3/d and 10,000 m^3/d permeate flow rate. The cost was broken down into CAPEX and OPEX, then each cost was classified into four elements furthermore. The results were shown in Fig. 22 and Fig. 23. Compared with conventional seawater RO, batch RO showed a 15% reduction in membrane replacement cost due to inherent osmotic backwashing and fouling suppression. Steel and equipment costs are increased due to the need for tanks, additional pressure vessels, and larger pressure exchangers relative to conventional RO. For batch RO, the pressure vessels are expensive, but in terms of total cost, batch RO was expected to be the cheapest for seawater desalination.

6. Conclusions

This paper has reviewed how RO membrane element performance affects RO plant costs in conventional RO processes and in newly proposed processes, for both seawater and brackish water desalination.

The review of past literature shows that the impact of membrane permeability on energy consumption varies significantly depending upon model assumptions and operating conditions. These differences appear in the range of values produced by prior research. However, the conclusion of Cohen-Tanugi et al. in 2014, that increased membrane permeability cannot radically reduce energy consumption, remains valid.

In the recently-proposed batch RO processes, although increasing membrane water permeability decreases the

reduction of specific energy consumption, the opportunity to reduce the specific energy consumption by increasing membrane water permeability is greater in comparison to conventional RO.

Increasing membrane water permeability has the potential to decrease the membrane surface area, which is a function of the number of RO elements. However, if the membrane surface area is decreased, the average operating flux must be increased to maintain the permeate flow rate, and higher flux increases the risk of fouling. Therefore, in order to more accurately evaluate the influence of membrane area on RO plant cost, the effect of fouling must be considered as well.

This review has also considered a wide range of RO element performance factors, beyond permeability. Today, major parts of the RO system have been highly optimized, particularly the energy recovery devices. Further reduction in energy use and plant cost will be more dependent upon optimization around different operating conditions, such as feed water and permeate water quality, time-varying performance factors, and the local costs of electricity and land. These issues will drive improvements to element design, membrane anti-fouling properties and selectivity, pre-treatment methods, anti-fouling feed spacers, and real-time monitoring techniques. Therefore, much more precise modeling and validation of plant performance will be required.

One additional and important conclusion is that the role of chronological changes in membrane performance, including the effect of fouling, requires further study to gauge its impact on energy use and operation over long periods of time. Most of the literature is based on only initial operating conditions and does not consider the effect of the changes in RO membrane element performance over time that inevitably result from factors such as fouling. Since these effects cause the membrane element performance to fluctuate, the specific energy consumption also varies with time. Even if the total RO plant cost using one type of RO element is expected to be lower than for other types of RO element, the total plant cost for long-term operation may be different depending on the difference in tolerance to ageing or fouling. Therefore, chronological effects must be considered to more accurately predict the relationship between RO membrane element performance and RO plant cost.

References

[1] M.A. Eltawil, Z. Zhengming, L. Yuan, A review of renewable energy technologies integrated with desalination systems, Renewable and Sustainable Energy Reviews, 13 (2009) 2245-2262.

[2] J. Song, T. Li, L. Wright-Contreras, A.W.-K. Law, A review of the current status of small-scale seawater reverse osmosis desalination, Water International, 42 (2017) 618-631.

[3] J. Imbrogno, G. Belfort, Membrane desalination: where are we, and what can we learn from fundamentals?, Annu. Rev. Chem. Biomol. Eng., 7 (2016) 29-64.

[4] S.S. Shenvi, A.M. Isloor, A.F. Ismail, A review on RO membrane technology: developments and challenges, Desalination, 368 (2015) 10-26.

[5] Y. Cohen, R. Semiat, A. Rahardianto, A perspective on reverse osmosis water desalination: quest for sustainability, AIChE J., 63 (2017) 1771-1784.

[6] T. Oki, S. Kanae, Global hydrological cycles and world water resources, Science, 313 (2006) 1068-1072.

[7] L.F. Greenlee, D.F. Lawler, B.D. Freeman, B. Marrot, P. Moulin, Reverse osmosis desalination: water sources, technology, and today's challenges, Water Research, 43 (2009) 2317-2348.

[8] IDA Desalination Yearbook 2017-2018, Media Analytics Ltd., 2017.

[9] IDA Water Security Handbook 2018-2019, IDA, 2018.

[10] C. Fritzmann, J. Löwenberg, T. Wintgens, T. Melin, State-of-the-art of reverse osmosis desalination, Desalination, 216 (2007) 1-76.

[11] A.H. Haidari, S.G.J. Heijman, W.G.J. van der Meer, Optimal design of spacers in reverse osmosis, Separation and Purification Technology, 192 (2018) 441-456.

[12] C.E. Reid, E.J. Breton, Water and Ion Flow Across Cellulosic Membranes, Journal of Applied Polymer Science, 1 (1959) 133-143.

[13] K.P. Lee, T.C. Arnot, D. Mattia, A review of reverse osmosis membrane materials for desalination—Development to date and future potential, Journal of Membrane Science, 370 (2011) 1-22.

[14] D. Li, Y. Yan, H. Wang, Recent advances in polymer and polymer composite membranes for reverse and forward osmosis processes, Progress in Polymer Science, 61 (2016) 104-155.

[15] M. Kurihara, T. Sasaki, The Pursuits of Ultimate Membrane Technology including Low Pressure Seawater Reverse Osmosis Membrane developed by "Mega-ton Water System" Project, Journal of Membrane Science & Research, (2017) 157-173.

[16] Z. Yang, X.-H. Ma, C.Y. Tang, Recent development of novel membranes for desalination, Desalination, 434 (2018) 37-59.

[17] D.M. Warsinger, S. Chakraborty, E.W. Tow, M.H. Plumlee, C. Bellona, S. Loutatidou, L. Karimi, A.M. Mikelonis, A. Achilli, A. Ghassemi, L.P. Padhye, S.A. Snyder, S. Curcio, C. Vecitis, H.A. Arafat, J.H. Lienhard, A review of polymeric membranes and processes for potable water reuse, Progress in Polymer Science, 81 (2016) 209-237.

[18] C. Bartels, M. Hirose, H. Fujioka, Performance advancement in the spiral wound RO/NF element design, in: 2007 EDS Conference, Greece, 2007.

[19] J. Johnson, M. Busch, Engineering aspects of reverse osmosis module design, Desalination and Water Treatment, 15 (2010) 236-248.

[20] M. Wilf, C. Bartels, Integrated membrane desalination systems - current status and projected development, in: http://membranes.com/knowledgecenter/technical-papers/.

[21] Features of Reverse Osmosis, in: https://www.toraywater.com/knowledge/kno_001_02.html, Toray Industries, Inc.

[22] N. Voutchkov, Energy use for membrane seawater desalination – current status and trends, Desalination, 431 (2018) 2-14.
[23] V.R. Escajadillo, Impact and sensitivity of diverse parameters over the cost structure of reverse osmosis systems, in: Civil Engineering, Delft University of Technology, 2016.
[24] K. Fethi, Optimization of energy consumption in the 3300 m^3/d RO Kerkennah plant, Desalination, 157 (2003) 145-149.
[25] E. Fredkin, New concepts in energy savings and process control for desalination plants using reverse osmosis, Desalination, 65 (1987) 321-330.
[26] V.G. Gude, Energy consumption and recovery in reverse osmosis, Desalination and Water Treatment, 36 (2012) 239-260.
[27] A.D. Khawaji, I.K. Kutubkhanah, J.-M. Wie, Advances in seawater desalination technologies, Desalination, 221 (2008) 47-69.
[28] A. Muñoz Elguera, S.O. Pérez Báez, Elimination of chemical products in the pre-treatment section of Las Palmas III reverse osmosis desalination plant to control fouling, Desalination, 437 (2018) 164-174.
[29] A. Subramani, M. Badruzzaman, J. Oppenheimer, J.G. Jacangelo, Energy minimization strategies and renewable energy utilization for desalination: a review, Water Research, 45 (2011) 1907-1920.
[30] S. Haryati, A.B. Hamzah, P.S. Goh, M.S. Abdullah, A.F. Ismail, M.D. Bustan, Process intensification of seawater reverse osmosis through enhanced train capacity and module size – Simulation on Lanzarote IV SWRO plant, Desalination, 408 (2017) 92-101.
[31] T. Manth, M. Gabor, E. Oklejas Jr, Minimizing RO energy consumption under variable conditions of operation, Desalination, 157 (2003) 9-21.
[32] A. Anit, R. Franks, C. Bartels, S.V. (Vasu), A. Emmert, D. Birch, Design and operation of a hybrid RO system using energy saving membranes and energy recovery to treat southern California ground water, in: http://membranes.com/knowledgecenter/technical-papers/.
[33] Y. Du, L. Xie, Y. Wang, Y. Xu, S. Wang, Optimization of reverse osmosis networks with spiral-wound modules, Industrial & Engineering Chemistry Research, 51 (2012) 11764-11777.
[34] M. Kurihara, H. Yamamura, T. Nakanishi, S. Jinno, Operation and reliability of very high-recovery seawater desalination technologies by brine conversion two-stage RO desalination system, Desalination, 138 (2001) 191-199.
[35] Y.-Y. Lu, Y.-D. Hu, X.-L. Zhang, L.-Y. Wu, Q.-Z. Liu, Optimum design of reverse osmosis system under different feed concentration and product specification, Journal of Membrane Science, 287 (2007) 219-229.
[36] H.W. Pohland, Seawater desalination by reverse osmosis, Endeavour, 4 (1980) 141-147.
[37] A. Zhu, P.D. Christofides, Y. Cohen, Energy consumption optimization of reverse osmosis membrane water desalination sublect to feed salinity fluctuation, Ind. Eng. Chem. Res., 48 (2009) 9581–9589.
[38] K. Rahmawati, N. Ghaffour, C. Aubry, G.L. Amy, Boron removal efficiency from Red Sea water using different SWRO/BWRO membranes, Journal of Membrane Science, 423-424 (2012) 522-529.
[39] A.M. Farooque, A.T.M. Jamaluddin, A.R. Al-Reweli, P.A.M. Jalaluddin, S.M. Al-Marwani, A.A. Al-Mobayed, A.H. Qasim, Parametric analyses of energy consumption and losses in SWCC SWRO plants utilizing energy recovery devices, Desalination, 219 (2008) 137-159.
[40] W.R. Association, Seawater Desalination Costs, in, Water Reuse Association 2012.
[41] N. Ghaffour, T.M. Missimer, G.L. Amy, Technical review and evaluation of the economics of water desalination: Current and future challenges for better water supply sustainability, Desalination, 309 (2013) 197-207.
[42] V. Romero-Ternero, L. García-Rodríguez, C. Gómez-Camacho, Thermoeconomic analysis of a seawater reverse osmosis plant, Desalination, 181 (2005) 43-59.
[43] A. Jiang, H. Wang, Y. Lin, W. Cheng, J. Wang, A study on optimal schedule of membrane cleaning and replacement for spiral-wound SWRO system, Desalination, 404 (2017) 259-269.
[44] S.S. Madaeni, S. Samieirad, Chemical cleaning of reverse osmosis membrane fouled by wastewater, Desalination, 257 (2010) 80-86.
[45] Y. Mei, H. Li, H. Xia, On the cleaning procedure of reverse osmosis membrane fouled by steel wastewater, Korean Journal of Chemical Engineering, 33 (2016) 2668-2673.
[46] J.-W. Nam, S.-H. Hong, J.-Y. Park, H.-S. Park, H.-S. Kim, A. Jang, Evaluation of chemical cleaning efficiency of organic-fouled SWRO membrane by analyzing filtration resistance, Desalination and Water Treatment, 51 (2013) 6172-6178.
[47] C.Y. Tang, T.H. Chong, A.G. Fane, Colloidal interactions and fouling of NF and RO membranes: a review, Adv. Colloid Interface Sci., 164 (2011) 126-143.
[48] E.O. Fridjonsson, S.J. Vogt, J.S. Vrouwenvelder, M.L. Johns, Early non-destructive biofouling detection in spiral wound RO membranes using a mobile earth′s field NMR, Journal of Membrane Science, 489 (2015) 227-236.
[49] S. Marka, S. Anand, Feed substrates influence biofilm formation on reverse osmosis membranes and their cleaning efficiency, J Dairy Sci, 101 (2018) 84-95.
[50] S. Farhat, F. Kamel, Y. Jedoui, M. Kallel, The relation between the RO fouling membrane and the feed water quality and the pretreatment in Djerba Island plant, Desalination, 286 (2012) 412-416.
[51] J.W. Nam, J.Y. Park, J.H. Kim, Y.S. Lee, E.J. Lee, M.J. Jeon, H.S. Kim, A. Jang, Effect on backwash cleaning efficiency with TDS concentrations of circulated water and backwashing water in SWRO membrane, Desalination and Water Treatment, 43 (2012) 124-130.
[52] T. Yu, L. Meng, Q.B. Zhao, Y. Shi, H.Y. Hu, Y. Lu, Effects of chemical cleaning on RO membrane inorganic, organic and microbial foulant removal in a full-scale plant for

municipal wastewater reclamation, Water Res, 113 (2017) 1-10.
[53] R. Deqian, Cleaning and regeneration of membranes, Desalination, 62 (1987) 363-371.
[54] J.B. Wang, J.Y. Cheng, T. Shi, Q. Huang, X.W. He, Membrane fouling mechanism and its control in the treatment of brackish water with reverse osmosis process, Advanced Materials Research, 788 (2013) 268-274.
[55] S.A. Avlonitis, K. Kouroumbas, N. Vlachakis, Energy consumption and membrane replacement cost for seawater RO desalination plants, Desalination, 157 (2003) 151-158.
[56] M. Wilf, C. Bartels, Optimization of seawater RO systems design, Desalination, 173 (2005) 1-12.
[57] S. Akashah, M. Abdel-Jawad, M.M. Abdelbalim, J. Dabdab, Cost and economic analysis of Doha reverse osmosis plant (Kuwait), Desalination, 64 (1987) 65-82.
[58] D.C. Brandt, Seawater reverse osmosis - An economic alternative to distillation, Desalination, 52 (1985) 177-186.
[59] L. Gao, S. Yoshikawa, Y. Iseri, S. Fujimori, S. Kanae, An economic assessment of the global potential for seawater desalination to 2050, Water, 9 (2017).
[60] S.J. Judd, Membrane technology costs and me, Water Research, 122 (2017) 1-9.
[61] J.H. Lienhard, G.P. Thiel, D.M. Warsinger, L.D. Banchik, Low Carbon Desalination: Status and Research, Development, and Demonstration Needs, in: Report of a workshop conducted at the Massachusetts Institute of Technology in association with the Global Clean Water Desalination Alliance, MIT Abdul Latif Jameel World Water and Food Security Lab, 2016.
[62] T. Pankratz, Water Desalination Report -31 July 2017, in: Water Desalination Report, Media Analytics. , 2017.
[63] S. Rybar, M. Vodnar, F.L. Vartolomei, R.L. Méndez, J.B.L. Ruano, Experience with renewable energy source and SWRO desalination, in: IDA (Ed.) International Desalination Association World Congress.
[64] N.M. Wade, The effect of the recent energy cost increase on the relative water costs from RO and distillation plants, Desalination, 81 (1991) 3-18.
[65] A. Yechiel, Y. Shevah, Optimization of energy costs for SWRO desalination plants, Desalination and Water Treatment, 46 (2012) 304-311.
[66] D. Cohen-Tanugi, R.K. McGovern, S.H. Dave, J.H. Lienhard, J.C. Grossman, Quantifying the potential of ultra-permeable membranes for water desalination, Energy & Environ. Sci., 7 (2014) 1134-1141.
[67] J.R. Werber, A. Deshmukh, M. Elimelech, The critical need for increased selectivity, not increased water permeability, for desalination membranes, Environmental Science & Technology Letters, 3 (2016) 112-120.
[68] N.M. Mazlan, D. Peshev, A.G. Livingston, Energy consumption for desalination — A comparison of forward osmosis with reverse osmosis, and the potential for perfect membranes, Desalination, 377 (2016) 138-151.
[69] R.K. McGovern, J.H. Lienhard, On the asymptotic flux of ultrapermeable seawater reverse osmosis membranes due to concentration polarisation, Journal of Membrane Science, 520 (2016) 560-565.
[70] A. Shrivastava, S. Rosenberg, M. Peery, Energy efficiency breakdown of reverse osmosis and its implications on future innovation roadmap for desalination, Desalination, 368 (2015) 181-192.
[71] A. Zhu, P.D. Christofides, Y. Cohen, Effect of thermodynamic restriction on energy cost optimization of RO membrane water desalination, Ind. Eng. Chem. Res., 48 (2009) 6010–6021.
[72] B. Absar, S.E.M.L. Kadi, O. Belhamiti, Reverse osmosis modeling with the orthogonal collocation on finite element method, Desalination and Water Treatment, 21 (2010) 23-32.
[73] D. Attarde, M. Jain, P.K. Singh, S.K. Gupta, Energy-efficient seawater desalination and wastewater treatment using osmotically driven membrane processes, Desalination, 413 (2017) 86-100.
[74] A. Chaudhuri, A. Jogdand, Permeate flux decrease due to concentration polarization in a closed roto-dynamic reverse osmosis filtration system, Desalination, 402 (2017) 152-161.
[75] E. Dimitriou, P. Boutikos, E.S. Mohamed, S. Koziel, G. Papadakis, Theoretical performance prediction of a reverse osmosis desalination membrane element under variable operating conditions, Desalination, 419 (2017) 70-78.
[76] B. Gu, X.Y. Xu, C.S. Adjiman, A predictive model for spiral wound reverse osmosis membrane modules: The effect of winding geometry and accurate geometric details, Comput. Chem. Eng., 96 (2017) 248-265.
[77] L.-Y. Hung, S.J. Lue, J.-H. You, Mass-transfer modeling of reverse-osmosis performance on 0.5–2% salty water, Desalination, 265 (2011) 67-73.
[78] Y. Lu, A. Liao, Y. Hu, Optimization design of RO system for water purification, in: 11th International Symposium on Process Systems Engineering, Singapore, 2012, pp. 230-234.
[79] L. Malaeb, G.M. Ayoub, Reverse osmosis technology for water treatment: State of the art review, Desalination, 267 (2011) 1-8.
[80] H.-J. Oh, T.-M. Hwang, S. Lee, A simplified simulation model of RO systems for seawater desalination, Desalination, 238 (2009) 128–139.
[81] M. Taniguchi, M. Kurihara, S. Kimura, Behavior of a reverse osmosis plant adopting a brine conversion two-stage process and its computer simulation, Journal of Membrane Science, 183 (2001) 249–257.
[82] D. Van Gauwbergen, J. Baeyens, Modeling and scaleup of reverse osmosis separation, Environmental Engineering Science, 19 (2002) 37-45.
[83] D. Paul, Reformulation of the solution-diffusion theory of reverse osmosis, Journal of Membrane Science, 241 (2004) 371-386.
[84] C.P. Koutsou, S.G. Yiantsisa, A.J. Karabelas, A numerical and experimental study of mass transfer in spacer-filled channels: Effects of spacer geometrical characteristics and Schmidt number, Journal of Membrane Science, 326 (2009) 234-251.
[85] F. Li, W. Meindersma, A.B. de Haan, T. Reith, Optimization of commercial net spacers in spiral wound

membrane modules, Journal of Membrane Science, 208 (2002) 289-302.
[86] G. Schock, A. Miquel, Mass transfer and pressure loss in spiral wound modules, Desalination, 64 (1987) 339-352.
[87] J. Schwinge, P.R. Neal, D.E. Wiley, D.F. Fletcher, A.G. Fane, Spiral wound modules and spacers Review and analysis, Journal of Membrane Science, 242 (2004) 129-153.
[88] A. Shrivastava, S. Kumar, E.L. Cussler, Predicting the effect of membrane spacers on mass transfer, Journal of Membrane Science, 323 (2008) 247-256.
[89] V. Geraldes, N.E. Pereira, M.N. de Pinho, Simulation and optimization of medium-sized seawater reverse osmosis processes with spiral-wound modules, Ind. Eng. Chem. Res., 44 (2005) 1897-1905.
[90] M. Li, Reducing specific energy consumption in Reverse Osmosis (RO) water desalination: An analysis from first principles, Desalination, 276 (2011) 128-135.
[91] A.J. Karabelas, C.P. Koutsou, M. Kostoglou, D.C. Sioutopoulos, Analysis of specific energy consumption in reverse osmosis desalination processes, Desalination, 431 (2018) 15-21.
[92] T.H. Chong, S.-L. Loo, W.B. Krantz, Energy-efficient reverse osmosis desalination process, Journal of Membrane Science, 473 (2015) 177-188.
[93] A.A. Mabrouk, A.S. Nafey, H.E.S. Fath, Thermoeconomic analysis of some existing desalination processes, Desalination, 205 (2007) 354-373.
[94] C. Liu, K. Rainwater, L. Song, Energy analysis and efficiency assessment of reverse osmosis desalination process, Desalination, 276 (2011) 352-358.
[95] C. Liu, K. Rainwater, L. Song, Calculation of energy consumption for crossflow RO desalination processes, Desalination and Water Treatment, 42 (2012) 295-303.
[96] B.J. Feinberg, G.Z. Ramon, E.M. Hoek, Thermodynamic analysis of osmotic energy recovery at a reverse osmosis desalination plant, Environ Sci Technol, 47 (2013) 2982-2989.
[97] M. Li, Energy consumption in spiral-wound seawater reverse osmosis at the thermodynamic limit, Industrial & Engineering Chemistry Research, 53 (2014) 3293-3299.
[98] S. Lin, M. Elimelech, Staged reverse osmosis operation: Configurations, energy efficiency, and application potential, Desalination, 366 (2015) 9-14.
[99] S. Lin, M. Elimelech, Kinetics and energetics trade-off in reverse osmosis desalination with different configurations, Desalination, 401 (2017) 42-52.
[100] F. Macedonio, E. Drioli, An exergetic analysis of a membrane desalination system, Desalination, 261 (2010) 293-299.
[101] A. Al-Zahrani, J. Orfi, Z. Al-Suhaibani, B. Salim, H. Al-Ansary, Thermodynamic analysis of a reverse osmosis desalination unit with energy recovery system, Procedia Engineering, 33 (2012) 404-414.
[102] X. Wang, Y. Tang, Exergetic analysis on the two-stage reverse osmosis seawater desalination system, Desalination and Water Treatment, 51 (2013) 2862-2870.
[103] A.M. Blanco-Marigorta, A. Lozano-Medina, J.D. Marcos, The exergetic efficiency as a performance evaluation tool in reverse osmosis desalination plants in operation, Desalination, 413 (2017) 19-28.
[104] T. Goda, S. Tai, A.N. Yamane, Evaluation of thermodynamical efficiency of reverse osmosis process using entropy, Water Research, 15 (1981) 1305-1311.
[105] M. Busch, W.E. Mickols, Reducing energy consumption in seawater desalination, Desalination, 165 (2004) 299-312.
[106] M. Wilf, Effect of new generation of low pressure, high salt rejection membranes on power consumption of RO systems, in: http://membranes.com/knowledgecenter/technical-papers/.
[107] R. Franks, C.R. Bartels, K. Andes, M. Patel, T.X. Yong, Implementing energy saving RO technology in large scale wastewater treatment plants, in: IDA World Congress-Maspalomas, Spain, 2007.
[108] M.C. Garg, H. Joshi, Optimization and economic analysis for a small scale nanofiltration and reverse osmosis water desalination system, Water Science and Technology: Water Supply, 15 (2015) 1027-1033.
[109] A. Zhu, P.D. Christofides, Y. Cohen, On RO membrane and energy costs and associated incentives for future enhancements of membrane permeability, Journal of Membrane Science, 344 (2009) 1-5.
[110] B. Shi, P. Marchetti, D. Peshev, S. Zhang, A.G. Livingston, Will ultra-high permeance membranes lead to ultra-efficient processes? Challenges for molecular separations in liquid systems, Journal of Membrane Science, 525 (2017) 35-47.
[111] Q.J. Wei, R.K. McGovern, J.H. Lienhard, Saving energy with an optimized two-stage reverse osmosis system, Environmental Science: Water Research & Technology, 3 (2017) 659-670.
[112] M. Wilf, Design consequences of recent improvements in membrane performance, Desalination, 113 (1997) 157-163.
[113] C.R. Bartels, K. Andes, Consideration of energy savings in SWRO, Desalination and Water Treatment, 51 (2013) 717-725.
[114] A. Zhu, P.D. Christofides, Y. Cohen, Minimization of energy consumption for a two-pass membrane desalination: Effect of energy recovery, membrane rejection and retentate recycling, Journal of Membrane Science, 339 (2009) 126-137.
[115] A. Zhu, A. Rahardianto, P.D. Christofides, Y. Cohen, Reverse osmosis desalination with high permeability membranes — Cost optimization and research needs, Desalination and Water Treatment, 15 (2012) 256-266.
[116] M. Elimelech, W.A. Phillip, The future of seawater desalination: energy, technology, and the environment, Science, 333 (2011) 712-717.
[117] L. Song, J.Y. Hu, S.L. Ong, W.J. Ng, M. Elimelech, M. Wilf, Emergence of thermodynamic restriction and its implications for full-scale reverse osmosis processes, Desalination, 155 (2003) 213-228.
[118] R. Franks, C. Bartels, M. Patel, Demonstrating improved RO membrane performance when reclaiming secondary manucipal waste, in: http://membranes.com/knowledgecenter/technical-papers/.

[119] J.H. Lienhard, K.H. Mistry, M.H. Sharqawy, G.P. Thiel, Thermodynamics, Exergy, and Energy Efficiency in Desalination Systems, in: Desalination Sustainability: A Technical, Socioeconomic, and Environmental Approach, Chapt. 4, Elsevier Publishing Co., 2017.
[120] K.H. Mistry, R.K. McGovern, G.P. Thiel, E.K. Summers, S.M. Zubair, J.H. Lienhard, Entropy Generation Analysis of Desalination Technologies, Entropy, 13 (2011) 1829-1864.
[121] L.A. Bromley, D. Singh, P. Ray, S. Sridhar, S.M. Read, Thermodynamic Properties of Sea Salt Solutions, AIChE J., 20 (1974) 326-335.
[122] R.W. Stoughton, M.H. Lietzke, Calculation of Some Thermodynamic Properties of Sea Salt Solutions at Elevated Temperatures from Data on NaCl Solutions, Journal of Chemical and Engineering Data, 10 (1965).
[123] E.M.V. Hoek, A.S. Kim, M. Elimelech, Influence of crossflow membrane filter geometry and shear rate on colloidal fouling in reverse osmosis and nanofiltration separations, Environmental Engineering Science, 19 (2002) 357-372.
[124] OLI Analyzer Studio Version 3.1, in, OLI systems, Inc., 2010.
[125] H. R., Physical electrochemistry of strong electrolytes based on partial dissociation and hydration, J. Electrochem. Soc., 143 (1996) 1789-1793.
[126] Q.J. Wei, R.K. McGovern, J.H. Lienhard V, Saving energy with an optimized two-stage reverse osmosis system, Environmental Science: Water Research & Technology, 3 (2017) 659-670.
[127] K.S. Pitzer, Ionic fluids, J. Phys. Chem. , 88 (1984) 2689-2697.
[128] G.P. Thiel, E.W. Tow, L.D. Banchik, H.W. Chung, J.H. Lienhard, Energy consumption in desalinating produced water from shale oil and gas extraction, Desalination, 366 (2015) 94-112.
[129] C.P. Koutsou, A.J. Karabelas, T.B. Goudoulas, Characteristics of permeate-side spacers of spiral wound membrane modules, Desalination, 322 (2013) 131-136.
[130] K. Jeong, M. Park, S.J. Ki, J.H. Kim, A systematic optimization of Internally Staged Design (ISD) for a full-scale reverse osmosis process, Journal of Membrane Science, 540 (2017) 285-296.
[131] P.K. Park, S. Lee, J.S. Cho, J.H. Kim, Full-scale simulation of seawater reverse osmosis desalination processes for boron removal: Effect of membrane fouling, Water Res, 46 (2012) 3796-3804.
[132] A.J. Karabelas, C.P. Koutsou, M. Kostoglou, The effect of spiral wound membrane element design characteristics on its performance in steady state desalination — A parametric study, Desalination, 332 (2014) 76-90.
[133] C.C. Zimmerer, V. Kottle, Effects of spacer geometry on pressure drop, mass transfer, mixing behavior, and residence time distribution, Desalination, 104 (1996) 129-134.
[134] C.P. Koutsou, S.G. Yiantsios, A.J. Karabelas, Direct numerical simulation of flow in spacer-filled channels: Effect of spacer geometrical characteristics, Journal of Membrane Science, 291 (2007) 53-69.
[135] A. Saeed, R. Vuthaluru, Y. Yang, H.B. Vuthaluru, Effect of feed spacer arrangement on flow dynamics through spacer filled membranes, Desalination, 285 (2012) 163-169.
[136] S.K. Karode, A. Kumar, Flow visualization through spacer filled channels by computational fluid dynamics Ⅰ. Pressure drop and shear rate calculations for flat sheet geometry, Journal of Membrane Science, 193 (2001) 69–84.
[137] J. Schwinge, D.E. Wiley, A.G. Fane, Novel spacer design improves observed flux, Journal of Membrane Science, 229 (2004) 53-61.
[138] M.A. Al-Obaidi, C. Kara-Zaïtri, I.M. Mujtaba, Significant energy savings by optimising membrane design in the multi-stage reverse osmosis wastewater treatment process, Environmental Science: Water Research & Technology, 4 (2018) 449-460.
[139] S.F. Rak, Reverse osmosis membrane module, in, United States, 1974.
[140] A.L. Ahmad, K.K. Lau, M.Z.A. Bakar, S.R.A. Shukor, Integrated CFD simulation of concentration polarization in narrow membrane channel, Comput. Chem. Eng., 29 (2005) 2087-2095.
[141] G.A. Fimbres-Weihs, D.E. Wiley, Numerical study of mass transfer in three-dimensional spacer-filled narrow channels with steady flow, Journal of Membrane Science, 306 (2007) 228-243.
[142] V. Geraldesa, V. Semigob, M.N. de Pinho, The effect of the ladder type spacers configuration in NF spiral-wound modules on the concentration boundary layers disruption, Desalination, 146 (2002) 187-194.
[143] M. Gimmelshtein, R. Semiat, Investigation of flow next to membrane walls, Journal of Membrane Science, 264 (2005) 137-150.
[144] A.J. Karabelas, Key issues for improving the design and operation of spiral-wound membrane modules in desalination plants, Desalination and Water Treatment, 52 (2013) 1820-1832.
[145] W.S. Kim, J.K. Park, H.N. Changs, Mass transfer in a three dimensional net type turbulance promoter, Int .J. Heat Mass Transfer, 30 (1987) 118-1192.
[146] Y.Y. Liang, G.A. Fimbres Weihs, D.E. Wiley, CFD modelling of electro-osmotic permeate flux enhancement in spacer-filled membrane channels, Journal of Membrane Science, 507 (2016) 107-118.
[147] S.Y. Lim, Y.Y. Liang, G.A. Fimbres Weihs, D.E. Wiley, D.F. Fletcher, A CFD study on the effect of membrane permeance on permeate flux enhancement generated by unsteady slip velocity, Journal of Membrane Science, 556 (2018) 138-145.
[148] F. Zamani, J.W. Chew, E. Akhondi, W.B. Krantz, A.G. Fane, Unsteady-state shear strategies to enhance mass-transfer for the implementation of ultrapermeable membranes in reverse osmosis: A review, Desalination, 356 (2015) 328-348.
[149] P.A. Araújo, D.J. Miller, P.B. Correia, M.C.M. van Loosdrecht, J.C. Kruithof, B.D. Freeman, D.R. Paul, J.S. Vrouwenvelder, Impact of feed spacer and membrane

modification by hydrophilic, bactericidal and biocidal coating on biofouling control, Desalination, 295 (2012) 1-10.
[150] P. Bacchin, P. Aimar, R. Field, Critical and sustainable fluxes: Theory, experiments and applications, Journal of Membrane Science, 281 (2006) 42-69.
[151] W. Bates, C. Bartels, L. Polonio, Improvements in RO technology for difficult feed waters, in: http://membranes.com/knowledgecenter/technical-papers/.
[152] W.T. Bates, C. Bartels, R. Franks, Improvements in spiral wound RO and NF membrane & elements construction for high fouling feed water applications, in: AMTA, 2008.
[153] R. Franks, C. Bartels, M. Patel, Demonstrating improved RO system performance with new low differential (LD) technology, in: http://membranes.com/knowledgecenter/technical-papers/.
[154] R. Hausman, T. Gullinkala, I.C. Escobar, Development of copper-charged polypropylene feedspacers for biofouling control, Journal of Membrane Science, 358 (2010) 114-121.
[155] W. Li, X. Su, A. Palazzolo, S. Ahmed, E. Thomas, Reverse osmosis membrane, seawater desalination with vibration assisted reduced inorganic fouling, Desalination, 417 (2017) 102-114.
[156] P.R. Neal, H. Li, A.G. Fane, D.E. Wiley, The effect of filament orientation on critical flux and particle deposition in spacer-filled channels, Journal of Membrane Science, 214 (2003) 165-178.
[157] H.-G. Park, S.-G. Cho, K.-J. Kim, Y.-N. Kwon, Effect of feed spacer thickness on the fouling behavior in reverse osmosis process — A pilot scale study, Desalination, 379 (2016) 155-163.
[158] J.S. Vrouwenvelder, J. Buiter, M. Riviere, W.G. van der Meer, M.C. van Loosdrecht, J.C. Kruithof, Impact of flow regime on pressure drop increase and biomass accumulation and morphology in membrane systems, Water Res, 44 (2010) 689-702.
[159] J.S. Vrouwenvelder, M.C. Van Loosdrecht, J.C. Kruithof, A novel scenario for biofouling control of spiral wound membrane systems, Water Res, 45 (2011) 3890-3898.
[160] J.S. Vrouwenvelder, J.A.M. van Paassen, J.M.C. van Agtmaal, M.C.M. van Loosdrecht, J.C. Kruithof, A critical flux to avoid biofouling of spiral wound nanofiltration and reverse osmosis membranes: Fact or fiction?, Journal of Membrane Science, 326 (2009) 36-44.
[161] A. Malek, M.N.A. Hawlader, J.C. Ho, Design and economics of RO seawater desalination, Desalination, 105 (1996) 245-261.
[162] A.G. Pervov, A.P. Andrianov, R.V. Efremov, A.V. Desyatov, A.E. Baranov, A new solution for the Caspian Sea desalination: low-pressure membranes, Desalination, 157 (2003) 377-384.
[163] A. Ruiz-García, E. Ruiz-Saavedra, 80,000 h operational experience and performance analysis of a brackish water reverse osmosis desalination plant. Assessment of membrane replacement cost, Desalination, 375 (2015) 81-88.
[164] M. Vanoppen, G. Stoffels, C. Demuytere, W. Bleyaert, A.R. Verliefde, Increasing RO efficiency by chemical-free ion-exchange and Donnan dialysis: Principles and practical implications, Water Res., 80 (2015) 59-70.
[165] S. Sethi, M.R. Wiesner, Cost modeling and estimation of crossflow membrane filtration processes, Environmental Engineering Science, 17 (2000) 61-79.
[166] A. Suárez, P. Fernández, J. Ramón Iglesias, E. Iglesias, F.A. Riera, Cost assessment of membrane processes: A practical example in the dairy wastewater reclamation by reverse osmosis, Journal of Membrane Science, 493 (2015) 389-402.
[167] A. Efraty, Closed circuit desalination series no. 8: record saving of RO energy by SWRO-CCD without need of energy recovery, Desalination and Water Treatment, 52 (2013) 5717-5730.
[168] A. Efraty, Closed circuit desalination series no-9: theoretical model assessment of the flexible BWRO-CCD technology for high recovery, low energy and reduced fouling applications, Desalination and Water Treatment, 53 (2013) 1755-1779.
[169] A. Efraty, CCD Series No-15: simple design batch SWRO-CCD units of high recovery and low energy without ERD for wide range flux operation of high cost-effectiveness, Desalination and Water Treatment, 57 (2015) 9166-9179.
[170] A. Efraty, CCD Series no 23: Theoretical model performance of BWRO desalination with CCD and multi-stage PFD of identical four-element modules under the same conditions, Desalination and Water Treatment, 75 (2017) 1-9.
[171] A. Efraty, R.N. Barak, Z. Gal, Closed circuit desalination series no-2: new affordable technology for sea water desalination of low energy and high flux using short modules without need of energy recovery, Desalination and Water Treatment, 42 (2012) 189-196.
[172] R.L. Stover, Industrial and brackish water treatment with closed circuit reverse osmosis, Desalination and Water Treatment, 51 (2013) 1124-1130.
[173] P.A. Davies, A. Afifi, F. Khatoon, G. Kuldip, S. Javed, S.J. Khan, Double-‐acting batch-‐RO system for desalination of brackish water with high efficiency and high recovery, in: Desalination for the Environment − Clean Energy and Water, Rome, Italy, 2016.
[174] P.A. Davies, J. Wayman, C. Alatta, K. Nguyen, J. Orfi, Desalination system with efficiency approaching the theoretical limits, Desalination and Water Treatment (2016).
[175] T. Qiu, P.A. Davies, Comparison of Configurations for High-Recovery Inland Desalination Systems, Water, 4 (2012) 690-706.
[176] T.Y. Qiu, P.A. Davies, Longitudinal dispersion in spiral wound RO modules and its effect on the performance of batch mode RO operations, Desalination, 288 (2012) 1-7.
[177] J. Swaminathan, R. Stover, E.W. Tow, D.M. Warsinger, J.H. Lienhard, Effect of practical losses on optimal design of batch RO systems, The International Desalination Association World Congress on Desalination and Water Reuse 2017, (2017).
[178] D.M. Warsinger, J. Swaminathan, J.H. Lienhard, Ultrapermeable membranes for batch desalination maximum

desalination energy efficiency and cost analysis, The International Desalination Association World Congress, (2017).
[179] D.M. Warsinger, E.W. Tow, K.G. Nayar, L.A. Maswadeh, J.H. Lienhard, Energy efficiency of batch and semi-batch (CCRO) reverse osmosis desalination, Water Res, 106 (2016) 272-282.
[180] Q.J. Wei, C.I. Tucker, P.J. Wu, A.M. Trueworthy, E.W. Tow, J.H. Lienhard, Batch Reverse Osmosis: Experimental Results, Model Validation, and Design Implications, in: 2019 Membrane Technology Conference & Exposition, New Orleans, USA, 2019.
[181] J.R. Werber, A. Deshmukh, M. Elimelech, Can batch or semi-batch processes save energy in reverse-osmosis desalination?, Desalination, 402 (2017) 109-122.